UNIVERSITY OF CALIFORNIA, SAN DIEGO

Red Blood Cell Membrane-Cloaked Nanoparticles For Drug Delivery

A Thesis submitted in partial satisfaction of the requirements
for the degree Master of Science

in

Nanoengineering

by

Cody Westcott Carpenter

Committee in charge:

Professor Liangfang Zhang, Chair
Professor Michael Heller
Professor Darren Lipomi

2014

The Thesis of Cody Westcott Carpenter is approved, and it is acceptable in quality and form for publication on microfilm and electronically:

_____

_____

_____

Chair

University of California, San Diego

2014

EPIGRAPH

"You're off to great places!
Today is your day!
Your mountain is waiting.
So get on your way!"
-Dr. Seuss

TABLE OF CONTENTS

LIST OF FIGURES

ACKNOWLEDGEMENTS

I would like to acknowledge Professor Liangfang Zhang for his support as the chair of my committee. Over the course of the past four years, his guidance has proved to be invaluable.

Chapter 1, in full, is a reprint of the material as it appears in Nanoscale 2013. Hu,C-M.; Fang, R.; Luk, B.; Chen, K.; Carpenter, C.; Gao, W.; Zhang, K.; Zhang, L. are the co-authors of this material.

Chapter 2, in full, is a reprint of the material as it appears in Nanoscale 2014. Luk, B.; Hu, C-M.; Fang, R.; Dehaini, D.; Carpenter, C.; Gao, W.; Zhang, L. are the co-authors of this material.

Chapter 3, in full, is a reprint of the material as it appears in Nanomedicine 2013. Aryal, S.; Hu, C-M.; Fang, R.; Dehaini, D.; Carpenter, C.; Zhang, D-E.; Zhang L. are the co-authors of this material.

Chapter 4, in full, is a reprint of the material as it appears in Nanoscale 2013. Fang, R.; Hu, C-M.; Chen, K.; Luk, B.; Carpenter, C.; Gao, W.; Li, S.; Zhang, D-E.; Lu, W.; Zhang, L. are the co-authors of this material.

ABSTRACT OF THE THESIS

Red Blood Cell Membrane-Cloaked
Nanoparticles For Drug Delivery

by

Cody Westcott Carpenter

Master of Science in Nanoengineering

University of California, San Diego, 2014

Professor Liangfang Zhang, Chair

Herein we describe the development of the Red Blood Cell coated nanoparticle, RBC-NP. Purified natural erythrocyte membrane is used to coat drug-loaded poly(lactic-co-glycolic acid) (PLGA). Synthetic PLGA co-polymer is biocompatible and biodegradable and has already received US FDA approval for drug-delivery and diagnostics. This work looks specifically at the retention of immunosuppressive proteins

on RBC-NPs, right-sidedness of natural RBC membranes interfacing with synthetic polymer nanoparticles, sustained and retarded drug release of RBC-NPs as well as further surface modification of RBC-NPs for increased targeting of model cancer cell lines.

Introduction

Nano drug delivery systems demonstrating long-circulation *in vivo* have substantial clinical relevance as they display high potential for passive and active targeting as well as sustained systemic drug release without immune cell detection.[1-3] Polymeric nanoparticles carrying large drug payloads are one such solution for their enhanced permeability and retention (EPR) size effect at solid tumor sites.[2, 3] Further efforts have been made to manipulate the surface, shape and size for better targeting and macrophage evasion.[4-6] The leading standard is to coat polymeric nanoparticles in poly(ethylene)-glycol (PEG), creating a stealthy hydration shell capable of relatively low immune detection.[2, 3] PEG coated formulations such as Doxil have shown clinical success, however recent reports of anti-PEG immune responses call for the exploration of other stealthy moieties to modify the surface of polymeric synthetic nanoparticles.[7]

Nature's long-circulating delivery vehicles, red blood cells (RBCs), are a model carrier for drug delivery systems. New techniques have lead scientists and nanotechnologists to mimic nature's RBCs structure and surface proteins to evade macrophage detection and subsequent clearance from the blood stream.[10-12] The merging of synthetic nanoparticles and natural biological moieties, such as, lipids and proteins fuel current research.[10-12]

Surface modification of synthetic nanoparticles through conjugation of the natural immunosuppressive protein CD47, found on RBCs, show a reduction in macrophage uptake of polystyrene beads.[11] However, such techniques cannot completely emulate the fluid mosaic structure and complex biochemistry of RBC membranes in their entirety and

rely on conjugation techniques vulnerable to protein denaturing. Currently, hijacking the complete RBC membrane and leveraging its natural surface characteristics as a delivery vehicle is being explored. This work focuses on the development of the RBC-NP platform.

References

1 Moghimi SM, Hunter AC, Murray JC (2001) Long-circulating and target-specific nanoparticles: Theory to practice. *Pharmacol Rev* 53:283-318.

2 Davis ME, Chen ZG, Shin DM (2008) Nanoparticle therapeutics: An emerging treatment modality for cancer. *Nat Rev Drug Discov* 7:771-782.

3 Peer D, Karp JM, Hong S, Farokhzad OC, Margalit R, Langer R (2007) Nanocarriers as an emerging platform for cancer therapy. *Nat Nanotechnol* 2:751-760.

4 Yoo JW, Chambers E, Mitragotri S (2010) Factors that control the circulation time of nanoparticles in blood: Challenges, solutions and future prospects. *Curr Pharm Des* 16:2298-2307.

5 Geng Y, Dalhaimer P, Cai S, Tsai R, Tewari M, Minko T, Discher DE (2007) Shape effects of filaments versus spherical particles in flow and drug delivery. *Nat Nanotechnol* 2:249-255.

6 Alexis F, Pridgen E, Molnar LK, Farokhzad OC (2008) Factors affecting the clearence and biodistribution of polymeric nanoparticles. *Mol Pharmacol* 5:505-515.

7 Knop K, Hoogenboom R, Fischer D, Schubert US (2010) Poly(ethylene glycol) in drug delivery: Pros and cons as well as potential alternatives. *Angew Chem Int Ed Engl* 49:6288-6308.

8 Jiang SY, Cao ZQ (2010) Ultra-fouling, functionalizable, and hydrolyzable zwitterionic materials and their derivatives for biological applications. *Adv Mater* 22:920-932.

9 Yang W, Zhang L, Wang S, White AD, Jiang S (2009) Functionizable and ultra stable nanoparticles coated with zwitterionc poly(carboxybetaine) in undiluted blood serum. *Biomaterials* 30:5617-5621.

10 Doshi N, Zahr AS, Bhaskar S, Lahann J, Mitragotri S (2009) Red blood cell-mimicking synthetic biomaterial particles. *Proc Natl Acad Sci USA* 106:21495-21499.

11 Tsai RK, Rodriguez PL, Discher DE (2010) Self inhibition of phagocytosis: The affinity of ‘marker of self’ CD47 for SIRPalpha dictates potency of inhibition but only at low expression levels. *Blood Cells Mol Dis* 45:67-74.

12 Merkel TJ, Jones SW, Herlihy KP, Kersey FR, Shields AR, Napier M, Luft JC, Wu H, Zamboni WC, Wang AZ, Bear JE, DeSimone JM (2011) Using mechanobiological mimicry of red blood cells to extend ciculation times of hydrogel microparticles. *Proc Natl Acad Sci USA* 108:586-591.

1 'Marker-of-self' functionalization of nanoscale particles through a top-down cellular membrane coating approach

*Nanoscale 2013

1.1 Introduction

We investigate the 'marker-of-self' functionalization of nanoparticles through coating of natural RBC membranes. The membrane translocation approach is shown to be highly efficient and bestows nanoparticles with correctly oriented and functional immunomodulatory CD47 at equivalent density to natural RBCs.

Enabling active immune evasion through biomimetic surface functionalization presents an emerging stealth strategy for developing long-circulating delivery vehicles.[1, 2] The identification of CD47, a transmembrane protein that serves as a universal molecular 'marker-of-self', has led to its utilization in the growing development of bio-inspired, immune-evasive devices. Capable of inhibiting phagocytosis and conferring anti-inflammatory properties through interactions with signal regulatory protein alpha (SIRPα) expressed by macrophages, CD47 and its analogs have been found to contribute to the *in vivo* survival of red blood cells (RBCs),[3] cancer cells,[4] and viruses[5]. Application of CD47 to modulate the immune responses against synthetic devices was first demonstrated with macrophages treated by purified recombinant, soluble CD47, which showed reduced uptake of colloidal emulsions.[6] Synthetic materials covalently conjugated with recombinant CD47 further advanced this biomimetic stealth approach, yielding polymeric microspheres[7] and implant surfaces with reduced affinity to inflammatory cells.[8, 9] On nanoscale particles, however, interfacing with native biological

components through chemical conjugation of immunomodulatory proteins to particle surfaces can be difficult to manipulate. In particular, inconsistent protein surface density and randomized ligand orientations are notable issues that can greatly undermine the performance of the resulting nanocarriers.

Toward engineering nanocarriers that can actively suppress immune attack by macrophages, herein we demonstrate a robust 'top-down' approach to functionalizing nanoscale particles with native CD47 by cloaking sub-100 nm nanoparticles with cellular membranes derived directly from natural RBCs (Figure 1). The uniqueness of this membrane coating approach lies in its ability to functionalize nanoparticles with native immunomodulatory proteins including CD47 at an equivalent density to that on natural RBCs. In this study, we show direct evidence that the 'marker-of-self' proteins are transferred to the particle surfaces and present in the right-side-out orientation. A macrophage uptake study confirms the stealth functionality conferred by the immunomodulatory proteins. Since cellular membranes anchor the many molecular tags that define cellular identities, attaching these membranes to nanoparticle surfaces provides unparalleled control over the functionalization of synthetic nanocarriers toward biomimicry.

With five membrane-spanning regions, CD47 is an integral membrane protein firmly embedded in RBC membranes, exhibiting an IgV-like extracellular domain that helps maintain the RBCs' survival in the circulation.[10] While it was previously shown that RBC membrane coating associated nanoparticles with the majority of the membrane materials,[11] it remained to be investigated whether these RBC membrane-coated nanoparticles (RBC-NPs) properly present the CD47 for immunomodulation.

Verification of the protein, its density, and its orientation on the RBC-NP surfaces demands a molecular examination of these RBC-mimicking nanocarriers. To investigate the functionalization of native CD47 on RBC-NPs, 70 nm poly(lactic-co-glycolic acid) (PLGA) particles were first extruded with RBC membrane-derived vesicles following a previously described protocol.[11] Through scanning electron microscopy (SEM) visualization, a spherical morphology was observed for the resulting RBC-NPs (Figure 2A), and dynamic light scattering measurements showed a mean particle diameter of 85 ± 2 nm (Supplement Figure S1). The purified particles were then solubilized in a lithium dodecyl sulphate (LDS) sample loading buffer, following which the protein contents stripped from the nanoparticles were separated by SDS-PAGE. The resulting protein gel was subsequently subjected to western blotting using anti-CD47 antibody as the primary immunostain. The presence of CD47 on the RBC-NPs was confirmed by a distinct, single band at 50 kDa (Figure 2B), which is the characteristic molecular weight of the CD47 protein self-marker.[10]

To further examine the extent of CD47 protein on the particle surfaces, the RBC-NPs prepared with different RBC membrane to polymeric particle ratios were collected and analysed for retained CD47 contents. An ultracentrifugation process was applied to isolate the resulting RBC-NPs from free RBC membranes, following which protein contents on the nanoparticles was processed through SDS-PAGE and examined by western blotting analysis. Figure 2C shows the relative CD47 retention on the different particle formulations. As the RBC membrane to polymeric particle ratio increased from 25 to 150 μL of blood per mg of polymer, a corresponding increase in the CD47 intensity was observed. This positive correlation reflects the increasing particle functionalization

by the increasing RBC membrane inputs, as more CD47 could be identified in the isolated nanoparticle samples. Saturation in CD47 band intensity was observed upon further raising the RBC membrane to polymer ratio above 150 μL/mg, which reflected the upper limit of CD47 functionalization achievable by the RBC membrane coating. To quantitatively analyze the protein density on the RBC-NPs, CD47 standards were prepared from predetermined volumes of blood, from which CD47 content was estimated based on the average CD47 number on a mouse RBC (16,500 copies per cell)[12] and the RBC concentration in mouse blood (10^{10} cells per mL of blood)[13] (Supplement discussion and Figure S2). Comparing the CD47 retention from the different RBC-NP formulations to the protein standards showed that the saturation level corresponded to approximately 2×10^{13} copies of CD47 per mg of polymeric particles (Figure 2D), yielding on average ~5 copies of CD47 per RBC-NP (Supplement discussion). To put the CD47 density into perspective, the surface area of the 85 nm RBC-NPs was calculated (~1×10^{11} μm^2/mg, Supplement discussion), from which a surface density of ~200 molecules of CD47 per μm^2 at saturation on the RBC-NPs can be derived. Given that natural RBCs possess 200~250 copies of CD47 per μm^2 [12, 14], the close match in the CD47 density on the RBC-NPs suggests that the membrane coating brought nearly all of RBCs' CD47 content onto the sub-100 nm particles. The result reflects the robustness of the membrane functionalization technique, as most of the membrane proteins were retained within the cellular membranes throughout the particle preparation process.

It should also be noted that the RBC membrane to polymer ratio corresponding to the onset of CD47 saturation was in close match to the theoretical ratio for complete unilamellar particle coating. Based on surface area estimations, approximately 125 μL of

blood is required to completely cover the surfaces of 1 mg of the 70 nm PLGA particles (Supplement discussion). Experimental observations showed that above the ratio of ~130 μL of blood/mg PLGA polymer, additional RBC membrane materials did not further functionalize the particles with CD47. As additional membrane materials in excess of complete unilamellar particle coverage were removed during the isolation of RBC-NPs, it can be inferred that the RBC membrane coating precluded further membrane interactions and that multilamellar membrane coating on the nanoparticles was unfavorable. To further investigate the RBC-NP formation under excessive RBC membrane to polymer ratios, RBC-NPs prepared with 250 μL of blood per mg of polymer were visualized under TEM (Supplement Figure S3). It was found that despite the availability of excess membrane materials in the samples, the nanoparticles were covered by a single, unilamellar coating of lipid membranes with a thickness of 6~8 nm, which is in agreement with the characteristic membrane thickness of RBCs.[15] Excess membranes remained in vesicular forms, which helped to explain the CD47 saturation on the RBC-NPs. In contrast to the unfavored multilamellar coating, unilamellar membrane coating on the RBC-NPs appeared to be highly efficient. By converting the RBC membrane input in Figure 2D to its corresponding CD47 content (Supplement Figure S4), the resulting correlation showed that, below the CD47 saturation, approximately 92% of the input membrane proteins were utilized for particle functionalization. This observation suggests that the RBC membrane coating to the PLGA particle surfaces was a favorable process that readily took place. The high efficiency in translocating CD47 onto nanoparticle surfaces confers a unique advantage to the RBC membrane coating approach.

To verify that the CD47 functionalized RBC-NPs possessed the properly oriented

self-markers for molecular interactions, the particle surfaces were examined for the presence of CD47's extracellular domains. Rat anti-CD47 antibodies specific to the CD47's extracellular region were applied to the RBC-NPs on a glow-discharged carbon-coated grid. Following 1 min of incubation, the sample was washed and subsequently incubated with anti-rat IgG gold conjugate, which labelled the anti-CD47 antibodies that were retained on the grid. The immunogold-labelled sample was then rinsed with water prior to visualization by transmission electron microscopy (TEM). Figure 3A shows the attachment of the electron-dense gold particles to multiple gray circular patterns 60-80 nm in diameter, which confirmed that the gold conjugates were attached to the RBC-NPs. A negative control prepared in the absence of the primary stain showed that the gold labelling was specific to the anti-CD47 antibodies (Supplement Figure S5). Together, these TEM results confirm the presence of right-side-out CD47 on the RBC-NPs. To further illustrate the CD47 functionalization by the RBC membrane coating, magnified images of RBC-NPs and the corresponding bare PLGA nanoparticles under negative staining or immunostaining are juxtaposed in Figure 3B. It can be observed that, following the RBC membrane coating, the particles were bestowed with a unilamellar membrane shell containing CD47 with correctly oriented extracellular domains for molecular interactions.

Lastly, the immunomodulatory effect of the CD47 functionalized RBC-NPs was studied. Bare PLGA nanoparticles and RBC-NPs loaded with hydrophobic DiD fluorophores (excitation/ emission = 644 nm/655 nm) were first incubated with J774 murine macrophage cells and examined for particle internalization. Following 10 min of incubation, the macrophage cells were washed and examined using flow cytometry,

which revealed that the RBC membrane coating rendered the particles less prone to the macrophage uptake, resulting in a 64% reduction in particle internalization (Figure 4). The reduced susceptibility to macrophage engulfment confirmed the translocation of immune-evasive functionality from RBCs to RBC-NPs and helped to explain the long *in vivo* circulation previously observed for the RBC-NPs.[11] To identify CD47's contribution to RBC-NPs' immune-evasive property, saturating amounts of anti-CD47 antibodies were applied to the RBC-NPs to block the right-side-out CD47 proteins. The antibody blocking was previously demonstrated to disrupt SIRPα signalling and increased macrophage engulfment of RBCs.[16] Similarly, depriving the particles of the molecular protection from phagocytosis resulted in an increase in particle internalization by 20%, which confirmed the immunomodulatory functionality conferred by theparticle-bound CD47. Curiously, the CD47-blocked RBC-NPs remained significantly more "stealthy" than the bare PLGA nanoparticles. Given that RBCs have a variety of proteins and glycans on their surface, many of which have been identified to modulate their immunological properties,[17, 18] other surface moieties in addition to CD47 on the RBC-NPs likely functioned collectively to inhibit the macrophage activity. Future studies are warranted to verify these other membrane moieties and to examine their implications in nanodevice functionalization.

1.2 Conclusions

In summary, RBC membrane coating was demonstrated to functionalize sub-100 nm substrates with native CD47, yielding nanoparticles with equivalent CD47 surface density to natural RBCs. Right-side-out CD47 proteins were identified on the particle surfaces, readily exposing their extracellular domain for molecular interactions. The

immune-evasive property of the RBC-NPs, as indicated by their reduced susceptibility to macrophage uptake, further verified the presence of functional immunomodulatory proteins on the particle surfaces. These biomimetic nanocarriers have tremendous potential in drug delivery applications, as they provide the opportunity to actively inhibit the immune clearance of their therapeutic cargo, thereby improving drug pharmacokinetics and therapeutic efficacy. The in-depth examination of the RBC-NPs also provides an up-close look at the fusion process between RBC membranes and PLGA polymeric particles, which appears to favour the formation of unilamellar membrane coated particles with the right-side-out membrane orientation. From synthesis and fabrication perspectives, the membrane coating technique contrasts with bottom-up functionalization schemes, which often employ chemical conjugation methods that can alter proteins' innate structures. The non-disruptive protein functionalization through the coating of natural cellular membranes presents a robust and versatile approach in interfacing synthetic materials with biological components, offering a compelling technique for the development of bio-inspired and biomimetic nanodevices.

Chapter 1, in full, is a reprint of the material as it appears in Nanoscale 2013. Hu,C-M.; Fang, R.; Luk, B.; Chen, K.; Carpenter, C.; Gao, W.; Zhang, K.; Zhang, L. are the co-authors of this material.

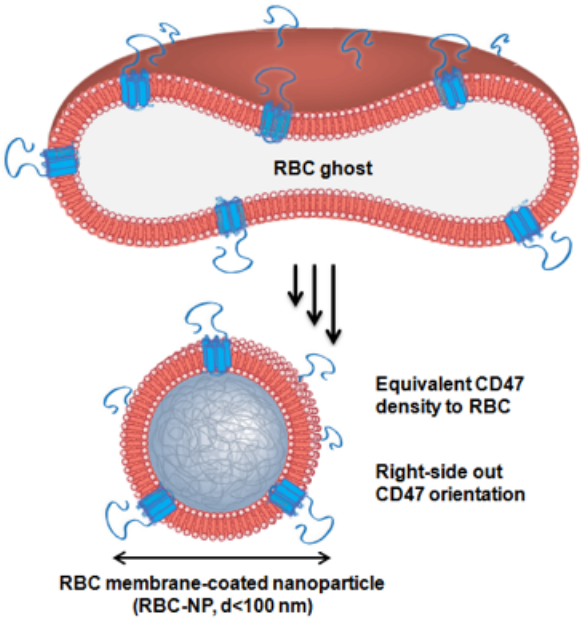

Figure 1.1. Schematic of controlled CD47 functionalization on nanoparticles enabled by RBC membrane coating. The resulting RBC membrane-coated nanoparticle (RBC-NP) has a CD47 density equivalent to that on a natural RBC.

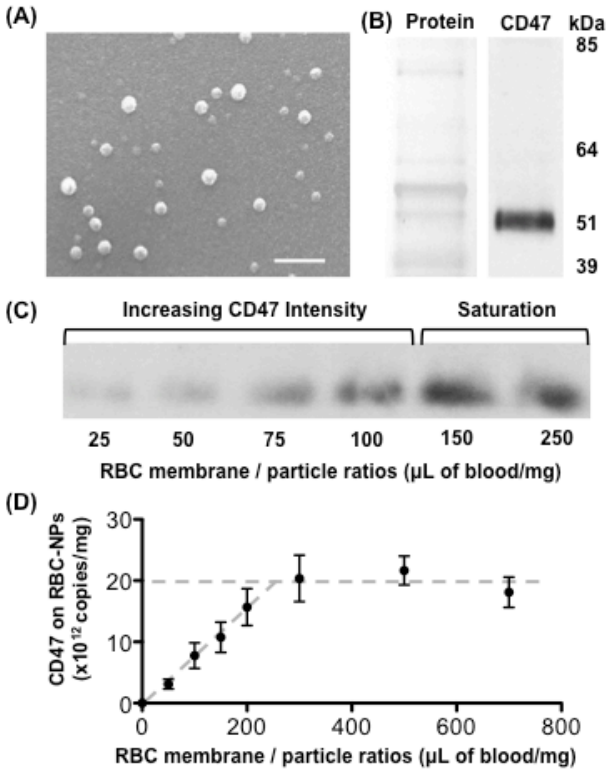

Figure 1.2. Characterization and quantification of CD47 on the RBC-NPs. (A) A representative scanning electron microscopy (SEM) image shows the spherical structure and morphology of the prepared RBC-NPs (scale bar = 250 nm). (B) Coomassie staining (left) and CD47 western blot (right) of the RBC-NPs' protein contents following SDS-PAGE separation. (C) Comparison of CD47 contents on the RBC-NPs prepared from different RBC membrane to polymer ratios. (D) Quantitative analysis of CD47 density on the RBC-NPs prepared from different RBC membrane to polymer ratios (n=5).

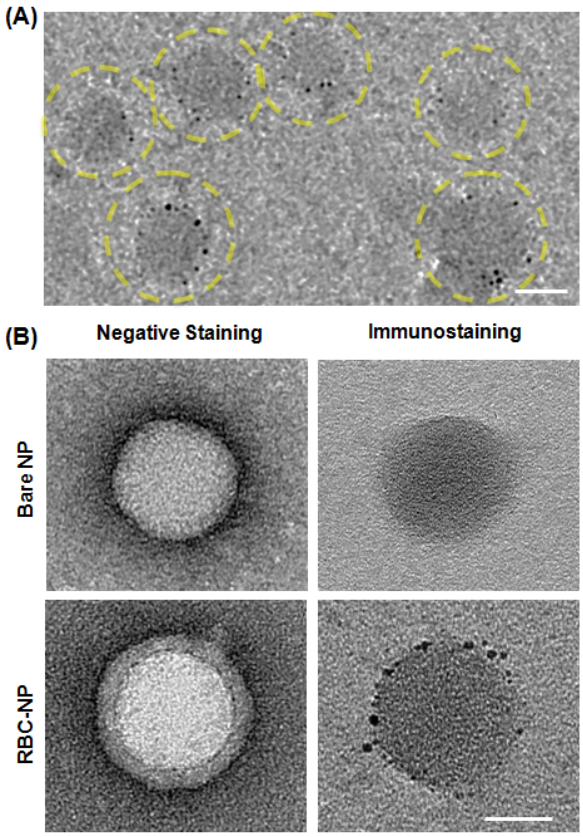

Figure 1.3. CD47 orientation on the RBC-NPs. (A) A representative transmission electron microscopy (TEM) image of the RBC-NPs under immunostaining, consisting of a primary stain by rat anti-mouse CD47 antibodies and a secondary stain by anti-rat IgG gold conjugates (scale bar = 50 nm). (B) Comparison of the RBC-NPs and the corresponding bare PLGA nanoparticles (bare NPs) and under negative staining with uranyl acetate or immunostaining (scale bar = 30 nm).

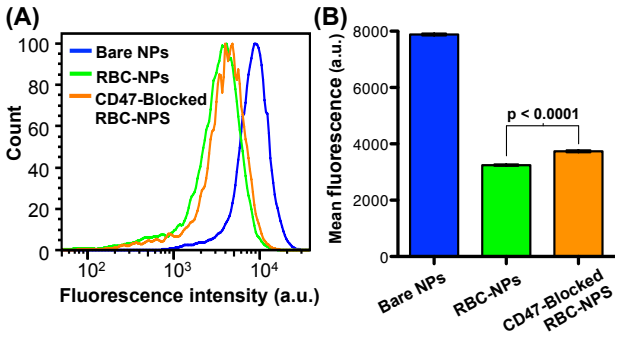

Figure 1.4. Inhibition of macrophage uptake. (A) Flow cytometry analysis of particle internalization by murine macrophage cells. The blue, green, and orange lines represent the bare PLGA nanoparticles (bare NPs), RBC-NPs, and CD47-blocked RBC-NPs, respectively. (B) Mean fluorescence intensity reflecting the overall particle uptake by the macrophage cells.

1.3 References

1 J. W. Yoo, D. J. Irvine, D. E. Discher and S. Mitragotri, *Nat Rev Drug Discov*, 2011, 10, 521-535.

2 S. C. Balmert and S. R. Little, *Adv Mater*, 2012, 24, 3757-3778.

3 P. A. Oldenborg, A. Zheleznyak, Y. F. Fang, C. F. Lagenaur, H. D. Gresham and F. P. Lindberg, *Science*, 2000, 288, 2051-2054.

4 S. Jaiswal, C. H. Jamieson, W. W. Pang, C. Y. Park, M. P. Chao, R. Majeti, D. Traver, N. van Rooijen and I. L. Weissman, *Cell*, 2009, 138, 271-285.

5 C. M. Cameron, J. W. Barrett, M. Mann, A. Lucas and G. McFadden, *Virology*, 2005, 337, 55-67.

6 Y. C. Hsu, M. Acuna, S. M. Tahara and C. A. Peng, *Pharm Res*, 2003, 20, 1539-1542.

7 R. K. Tsai, P. L. Rodriguez and D. E. Discher, *Blood Cells Mol Dis*, 2010, 45, 67-74.

8 M. J. Finley, L. Rauova, I. S. Alferiev, J. W. Weisel, R. J. Levy and S. J. Stachelek, *Biomaterials*, 2012, 33, 5803-5811.

9 S. J. Stachelek, M. J. Finley, I. S. Alferiev, F. Wang, R. K. Tsai, E. C. Eckells, N. Tomczyk, J. M. Connolly, D. E. Discher, D. M. Eckmann and R. J. Levy, *Biomaterials*, 2011, 32, 4317-4326.

10 E. J. Brown and W. A. Frazier, *Trends Cell Biol*, 2001, 11, 130-135.

11 C. M. Hu, L. Zhang, S. Aryal, C. Cheung and R. H. Fang, *Proc Natl Acad Sci U S A*, 2011, 108, 10980-10985.

12 S. Subramanian, R. Tsai, S. Sen, K. N. Dahl and D. E. Discher, *Blood Cells Mol Dis*, 2006, 36, 364-372.

13 E. S. Russell, E. F. Neufeld and C. T. Higgins, *Proc Soc Exp Biol Med*, 1951, 78, 761-766.

14 I. Mouro-Chanteloup, J. Delaunay, P. Gane, V. Nicolas, M. Johansen, E. J. Brown, L. L. Peters, C. L. Van Kim, J. P. Cartron and Y. Colin, *Blood*, 2003, 101, 338-344.

15 R. M. Hochmuth, C. A. Evans, H. C. Wiles and J. T. McCown, *Science*, 1983, 220, 101-102.

16 P. A. Oldenborg, H. D. Gresham and F. P. Lindberg, *J Exp Med*, 2001, 193, 855-862.

17 C. M. Hu, R. H. Fang and L. Zhang, *Advanced Healthcare Materials*, 2012, 1, 537-547.

18 J. R. Durocher, R. C. Payne and M. E. Conrad, *Blood*, 1975, 45, 11-20.

2 Interfacial Interactions between Natural RBC Membranes and Synthetic Polymeric Nanoparticles

*Nanoscale 2014

2.1 Introduction

Recent advancement in biology and materials engineering has led to surging interests in bio-inspired nanodevices with biomimetic functionalities.[1-3] Exploiting the immunomodulatory self-marker proteins commonly found on cells for nanocarrier functionalization has bestowed unique anti-phagocytic properties and prolonged *in vivo* survival onto nanoparticles.[4,5] Among bio-inspired nanocarriers, a recently developed RBC membrane-cloaked nanoparticle (RBC-NP) platform presents an intriguing system as it utilizes RBC membrane content in its entirety for immune-evasive stealth camouflage[6,7] and therapeutic purposes.[8,9] Upon unilamellar membrane coating, RBC-NPs display self-marker proteins with a right-side-out orientation bias,[10] which contributes to the prolonged *in vivo* circulation time of the platform. The unique structural features and properties of RBC-NPs raise curiosity concerning the biomembrane-particle interface that plays a significant role in enabling colloidal stability and preserving biomimetic functionalities of the platform. In this study, we dissect the RBC-NP system to shed light on the mechanisms that elegantly bridge synthetic polymeric particles with natural cellular membranes.

While the development of RBC-inspired drug carriers have focused primarily on mechano-mimicry[11-13] and protein functionalization,[5] the present study introduces a different emphasis on surface glycans, which in fact represent the predominant moieties

on cellular surfaces.[14] On RBCs, the dense glycan coatings, known as glycocalyx, have significant implications in the stabilization and immune-evasive properties of the cells.[15-19] These complex polysaccharides serve as a hydrophilic coating, and stabilizing strategies using analogous sugar polymers can be found in many carbohydrate-functionalized nanoformulations.[20-22] The asymmetric membrane distribution of glycans, which reside exclusively on the extracellular side of RBCs, also make glycans a good indicator of membrane sidedness.[23,24] In addition, the abundant, negatively charged sialyl residues at the glycan terminus bestow a charge asymmetry across cellular membranes,[25] which can affect interfacial interactions between RBC membranes and synthetic polymeric particles through electrostatic interactions. Herein, we carry out a series of studies to examine several interfacial aspects of RBC-NPs, including completeness of membrane coverage, membrane sidedness on the nanoparticles, and the effects of polymeric particles' surface charge and surface curvature on the membrane cloaking process. These studies help scrutinize the RBC-NP platform from a colloidal science perspective and shed light on the implications of membrane glycans and nanoparticle properties on RBC-NP formation. The studies also provide pertinent information toward future translation of the RBC-NP platform as well as inspirations for both synthetic and naturally derived nanoparticle designs.

2.2 Materials and Methods

2.2.1 Preparation and Characterization of RBC-NPs

RBC membranes were derived from whole blood collected from male imprinting control region (ICR) mice (Charles River Laboratories, Wilmington, MA). Whole blood was centrifuged and subjected to hemolysis by hypotonic treatment to isolate RBC

membranes. The membranes were then bath sonicated for 3 min using an FS30D bath sonicator (Fisher Scientific, Waltham, MA) at a frequency of 42 kHz and a power of 100W and subsequently extruded through a 100 nm polycarbonate porous membrane using an Avanti mini extruder to form RBC membrane vesicles. In parallel, poly($_{D,L}$-lactide-*co*-glycolide acid) (PLGA) polymeric cores were prepared using 0.67dL g^{-1} carboxy-terminated 50:50 PLGA polymer (LACTEL Absorbable Polymers, Birmingham, AL) through a solvent displacement method. PLGA was first dissolved in acetone at a concentration of 1mg mL^{-1} and added dropwise to 3 mL of water. The mixture was then stirred in open air for 2 h and filtered using an Amicon Ultra-4 Centrifugal Filter with a molecular weight cutoff (MWCO) of 10,000 Da (Millipore, Billerica, MA). To fuse the RBC membrane vesicles with the PLGA cores, 1 mg of PLGA particles was mixed with RBC membranes derived from various amounts of mouse whole blood and extruded through a 100 nm polycarbonate porous membrane using an Avanti mini extruder. The hydrodynamic diameter, polydispersity index, and surface zeta potential of the resulting RBC-NPs were determined from three repeated experiments using dynamic light scattering (DLS) on a ZEN3600 Nano Zetasizer (Malvern Instruments, UK) at 25ºC. Transmission electron microscopy (TEM) images were taken to examine the structure of the RBC-NPs. A drop of the RBC-NP solution at a concentration of 2 mg mL^{-1} was deposited onto a glow-discharged carbon-coated grid. After 5 min, the grid was rinsed with 10 drops of distilled water and a drop of 1% uranyl acetate stain was added for negative staining. The grid was then dried and imaged using a Tecnai G2 Sphera (FEI, Hillsboro, OR) microscope.

2.2.2 Membrane Coverage Assay

Biotin-functionalized PLGA was prepared by conjugating amine-PEG_2-biotin to 0.67 dL g^{-1} carboxy-terminated PLGA (Thermo Scientific, Waltham, MA). 100 mg of PLGA was dissolved in 2.5 mL chloroform and activated with 5 mg of ethyl(dimethylaminopropyl) carbodiimide (EDC) and 5.5 mg of N-hydroxysuccinimide (NHS) (Thermo Scientific, Waltham, MA). Following 60 min of activation, a 3-to-1 molar excess of amine-PEG_2-biotin was added to the polymer solution along with 8 μL of N,N-diisopropylethylamine (Fisher Scientific, Waltham, MA). After overnight incubation under gentle stirring, the polymer was precipitated by adding the solution dropwise into 40 mL of -20°C methanol. Functionalized PLGA was pelleted through centrifugation at 3500 rpm for 5 min. The pelleted polymer was then dissolved in chloroform and further purified in -20°C methanol two more times. Following the last wash, the biotin-functionalized PLGA was dried in vacuum and dissolved in acetone. For the preparation of biotin-functionalized PLGA particles, 1 mg mL^{-1} of PLGA solution containing 2% of biotin-PLGA was prepared in acetone and added dropwise to 3 mL of water. The mixture was then stirred in open air for 2 h and filtered using an Amicon Ultra-4 Centrifugal Filter with MWCO of 10,000 Da (Millipore, Billerica, MA). Biotin functionalization on nanoparticle surfaces was confirmed by incubating 1 mL of 1 mg mL^{-1} biotinylated nanoparticles with 20 μg of streptavidin (Invitrogen, Grand Island, NY) for 30 min. Particle aggregation induced by streptavidin-biotin interactions was monitored by DLS, using non-biotinylated PLGA particles as a negative control. The biotinylated PLGA particles were then used to examine the extent of particle surface coverage by RBC membranes. 1 mL of 1 mg mL^{-1} RBC-NPs prepared with different membrane-to-particle

ratios were incubated with 20 μg of streptavidin for 30 min. Particle size was determined from three repeated experiments using DLS at 25ºC.

2.2.3 Membrane Sidedness Assay

RBC-NPs were first prepared with 100 nm PLGA cores and RBC membrane vesicles. For glycoprotein quantification, proteins exposed on the RBC-NP surfaces were trypsinized by incubating 1 mL of 1 mg mL^{-1} RBC-NPs with 5 μg of trypsin (G-Biosciences, St. Louis, MO) at room temperature for 2 h. Sialic acid removal from RBC-NPs was performed by incubating 1 mL of 1 mg mL^{-1} of RBC-NPs in water with 100 units of sialidase (Roche Diagnostics, Indianapolis, IN) at room temperature for 2 h. The samples were then centrifuged at 200,000 × g for 45 min using an Optima L-90K Ultracentrifuge (Beckman Coulter, Brea, CA), and the supernatant was collected and examined for glycoprotein and sialic acid content. To quantify glycoprotein, the supernatant was examined using Glycoprotein Detection Reagent (Thermo Scientific) following manufacturer's instructions. To quantify sialic acid, the supernatant was examined using Sialic Acid Quantification Kit (Sigma-Aldrich, St. Louis, MO) following the manufacturer's instructions. Equivalent amounts of RBC ghosts and bare PLGA cores were used as a positive and a negative control, respectively.

2.2.4 Stability Study of RBC-NPs

A series of RBC-NP formulations were prepared by coating 1 mg of PLGA cores with RBC membranes collected from 200 μL, 100 μL, 75 μL, 50 μL, 25 μL or 0 μL of mouse blood. Each formulation was then adjusted to 1 × PBS buffer (pH = 7.4) and sonicated for 5 min using an FS30D bath sonicator (Fisher Scientific, Waltham, MA) at a frequency of 42 kHz and a power of 100W to facilitate the aggregation process. After

sonication, the hydrodynamic diameter of the particles was determined using DLS. Trypsinized RBC-NPs were prepared by incubating a stable RBC-NP formulation (100 μL blood per mg PLGA core) with 50 μg mL^{-1} trypsin (G-Biosciences, St. Louis, MO). Two hours following the trypsinization, the particle size was measured by DLS.

2.2.5 Preparation of RBC-NPs with Positively Charged Polymeric Cores

To create positively charged polymeric cores, 100 nm PLGA nanoparticles prepared using the aforementioned protocol were mixed with 5% (w/w) polyethylenimine (PEI, molecular weight = 1,800 Da) and bath sonicated for 5 min. The resulting nanoparticle solution was filtered using an Amicon Filter with MWCO of 10,000 Da. The hydrodynamic size, polydispersity index, and surface zeta potential of the PEI-coated PLGA particles were characterized by DLS. 1 mg of the resulting positively charged nanoparticles was then mixed with RBC membrane vesicles derived from 100 μL of whole blood and extruded through 200 nm, 400 nm or 1000 nm polycarbonate porous membrane using an Avanti mini extruder. The particle size and surface zeta potential before and after RBC membrane coating were measured by DLS. The structure of the particles was examined using TEM after negative staining with uranyl acetate.

2.2.6 Preparation of RBC-NPs with Differently Sized Polymeric Cores

Differently sized PLGA cores between 65 to 340 nm in diameter were prepared by adjusting the polymer concentration, the solvent-to-water ratio, and the ionic content in the aqueous phase during the nanoprecipitation process. Specifically, to make 65 nm PLGA cores, 1 mL of 5 mg mL^{-1} PLGA dissolved in acetone was pipetted into 3 mL of water. 120 nm cores were made by pipetting 1 mL of 10 mg mL^{-1} PLGA dissolved in acetone into 3 mL of water. 200 nm cores were made by pipetting 1 mL of 10 mg mL^{-}

[1]PLGA dissolved in acetone into 4 mL of 2.5 × PBS. 340 nm cores were made by adding water dropwise into 1 mL of 3 mg mL^{-1} PLGA dissolved in acetone until cloudiness was observed in the solution. All formulations were then evaporated in a vacuum chamber overnight to remove excess acetone. The prepared cores were washed 3 times using Amicon Filters with MWCO of 10,000 Da prior to coating with RBC membranes. A 10% excess of RBC membranes was added to each core type based on the theoretical membrane-to-polymer ratio for complete membrane coverage (Supporting Information). For 65 nm cores, RBC membranes derived from 165 μL of blood were added and the mixture was extruded through a 100 nm porous membrane. For 120 nm cores, RBC membranes derived from 75 μL of blood were added and the mixture was extruded through a 200 nm porous membrane. For 200 nm cores, RBC membranes derived from 40 μL of blood were added and the mixture was extruded through a 400 nm porous membrane. For 340 nm cores, RBC membranes derived from 23 μL of blood were added and the mixture was extruded through a 400 nm porous membrane. The particle size and zeta potential before and after RBC membrane coating were measured by DLS. The core-shell structure of the particles was examined using TEM after negative staining with uranyl acetate.

2.3 Results

2.3.1 Completeness of RBC Membrane Coverage

RBC-NPs were first examined for the completeness of the membrane coverage. An aggregation assay based on streptavidin/biotin cross-linking chemistry was implemented to examine whether polymeric surfaces were exposed. In the study, biotinylated poly($_{D,L}$-lactide-*co*-glycolide) (PLGA) nanoparticles were prepared, which

readily aggregate upon direct exposure to free streptavidin in solution (Fig. 1A). Carboxylated PLGA polymers were first functionalized with amine-PEG_2-biotin using EDC/NHS chemistry, and the resulting biotinylated PLGA polymers were mixed with carboxylated PLGA at a 1:50 ratio to form biotinylated polymeric nanoparticles. The biotin-conjugated polymers showed negligible effect on the physicochemical properties of the PLGA cores (ESI Fig. S1 and Fig. S2†), as both biotinylated and non-biotinylated particles were ~100 nm in size and -45 mV in surface zeta potential. Upon mixture with free streptavidin, the biotinylated cores aggregated to approximately 2,000 nm, whereas the non-biotinylated cores remained similar in size, demonstrating a particle bridging mechanism that was specific to the strong streptavidin-biotin interaction. A slight size increase by ~ 10 nm was observed in the non-biotinylated cores upon streptavidin mixture, which was likely due to the non-specific protein absorption on the particle surface.

Given that bilayer membranes can preclude surface-attached biotins from interacting with the 60 kDa streptavidin, the completeness of RBC membrane coating was then evaluated using the biotinylated polymeric cores. Using a previously described extrusion process,[6] the cores were coated with increasing amounts of RBC membrane content ranging from 0 to 350 μL of mouse blood per mg of polymer. The coated cores were then mixed with streptavidin and monitored for particle size change. At low membrane-to-polymer ratios (below 25 μL mg^{-1}), significant aggregation was observed. However, as membrane-to-polymer ratio increased to 100 μL mg^{-1} or higher, the addition of streptavidin failed to induce any considerable size increase among the biotinylated cores (Fig. 1B). The preclusion of streptavidin-induced aggregation suggests that the

particle surfaces were completely shielded, and 100 μL mg^{-1} was sufficient to fully coat all the nanoparticles present. Based on the particle surface area, RBC surface area, and RBC concentration in mouse blood, it was estimated that ~85 μL of mouse blood would be needed to derive enough RBC membrane material to completely coat 1 mg of 100 nm PLGA nanoparticles (Supporting Information). The close match between the theoretical and the experimental membrane-to-polymer ratio for full coverage suggests a high membrane coating efficiency, which is consistent with a previous study that showed a high protein translocation yield through the membrane coating approach.[10]

2.3.2 Sidedness of RBC Membranes upon Coating

Owing to the asymmetric distribution of glycans on the extracellular side of cellular membranes, these glycans can be used as an indicator to quantitatively analyze the membrane sidedness on RBC-NPs. A trypsinization method was herein applied to examine the glycoprotein content on the outer surface of RBC-NPs.[26] In the study, RBC-NPs were first prepared with excess polymeric cores to ensure that all RBC membranes were occupied. RBC ghosts containing equivalent amount of membrane content and bare polymeric cores were prepared as positive and negative controls, respectively. The samples were then trypsinized for 2 h and subjected to ultracentrifugation at 200,000 × g for 45 min. Since RBC bilayer membranes are impermeable to trypsin, membrane sidedness can be assessed by measuring the enzymatically removed glycoprotein content.[26] Detached glycoproteins were collected from the sample supernatant and quantified using a periodate-based glycoprotein detection assay (Fig. 2A). Relative to the glycoprotein content in trypsinized RBC ghosts, trypsinized RBC-NPs yielded ~95% of the glycoprotein content in the sample supernatant (Fig. 2B). This result indicates that the

majority of surface glycoproteins on RBC-NPs were exposed to the trypsin treatment, corroborating a right-side-out membrane orientation that was previously observed by immunogold staining of surface proteins.[10]

To further verify the membrane sidedness of RBC-NPs, a secondary assay was applied to quantify sialic acid, a characteristic carbohydrate terminus on RBC glycans. A sialidase enzyme was used to remove the terminal sialyl groups on the RBC-NPs (Fig. 2A). Unlike the complete glycoprotein removal by trypsin, sialidase treatment only removed the terminal carbohydrate and did not affect the size of the RBC-NPs (ESI Fig. S3A†). The enzymatic activity, however, could be observed through surface zeta potential measurements as the removal of negatively charged sialic acid altered the surface charge of the RBC-NPs. Following 2 h of sialidase treatment, the zeta potential of RBC-NPs shifted from -23 mV to -0.6 mV, whereas that for bare nanoparticles remained largely unchanged (ESI Fig. S3B†), verifying the enzymatic removal of sialic acid. Following sialidase treatment and ultracentrifugation at 200,000 × g, the sample supernatants were collected and assayed using a sialic acid quantification kit. It was found that per RBC membrane content derived from 1 mL of blood, 122 ± 8 and 112 ± 2 nmole of sialic acid was recovered from RBC ghosts and RBC-NPs, respectively (Fig. 2C). The values are consistent with reported sialic acid density on erythrocytes,[27] and the close match in sialic acid recovery further supports the right-side-out-membrane orientation of the RBC-NPs. Based on the quantification result, it can also be estimated that at full coverage each RBC-NP with 100 nm in core diameter possesses ~43,500 sialyl moieties (Supplementary Information). This dense population of surface sialyl moieties have strong implications on the RBC-NPs' properties as they are a key

modulator of cellular interaction and immune activation and contribute to erythrocytes' *in vivo* survival. [18,19,28]

2.3.3 RBC Membrane Cloaks Stabilizing Polymeric Cores

Upon verification that RBC membrane can completely envelop PLGA nanoparticles with a right-side-out membrane orientation, the stabilizing effect of the membrane coating was then evaluated. Carboxylated PLGA was used to prepare polymeric cores that were ~100 nm in diameter with a surface zeta potential of -45 mV. The cores were then extruded with various amounts of RBC membrane to form RBC-NPs. To test the stabilizing effect of RBC membranes, the particle solution was adjusted to 1 × PBS (pH = 7.4), in which non-stabilized nanoparticles are known to aggregate owing to the charge screening effect by the ionic environment. Following brief sonication to agitate the sample solutions, the nanoparticle sizes were monitored using dynamic light scattering (DLS). For the formulations containing 0, 25, 50, 75, 100, and 200 μL of RBC membrane per mg of PLGA core, the final particle sizes following sonication in PBS were 1965 ± 152 nm, 850 ± 84 nm, 395 ± 51 nm, 135 ± 2nm, 117 ± 1 nm, and 116 ± 2 nm respectively (Fig. 3A). The results reflect the increasing particle stability with higher RBC membrane content, and above 100 μL/mg of membrane-to-particle ratio, which is above the theoretical value for full particle coverage, the nanoparticles showed negligible size increase following sonication.

The stabilizing effect of RBC membranes can be attributed to the copious surface glycans present, which are highly hydrophilic and contribute to the steric stabilization of cells.[15,17] To examine the role of these glycans in enabling colloidal stability, stabilized RBC-NPs (membrane-to-polymer ratio: 100 μL blood per mg polymer) were treated with

trypsin, which enzymatically cleaves glycoproteins that serve to anchor the majority of RBC surface glycans. 2 h following trypsinization, significant RBC-NP aggregation was observed (Fig. 3B). The loss of colloidal stability following trypsinization suggests that the phospholipid membrane bilayer alone is not sufficient to stabilize the particles, and that steric stabilization was enabled by the polysaccharides on RBC membranes. The stabilizing capability of hydrophilic glycans is not surprising, as synthetic polysaccharides have been commonly applied for nanoparticle stabilization.[20-22] In the RBC-NP platform, polymeric nanoparticles are functionalized by naturally derived surface glycans. This glycan stabilization mechanism also provides an explanation to the efficient membrane cloaking process, in which unilamellar membrane coating readily occurs and yet multilamellar coating is not observed despite excess membrane materials (ESI Fig. S4†); the non-stabilized polymeric surfaces with higher surface energy would readily interact with glycan-stabilized membranes to minimize the overall energy, whereas glycan-stabilized RBC-NP surfaces preclude further membrane interactions.

2.3.4 Surface Charge of Polymeric Cores Affecting RBC Membrane Coating

To further advance the understanding and development of cell membrane-cloaked nanoparticles, we examined effects of the nanoparticle core properties on the formation of the RBC-NPs. Since electrostatic effect has shown strong influence on lipid membrane interactions with nanoparticle substrate,[29] we investigated the use of positively and negatively charged polymeric cores for RBC-NP preparations. The negatively charged cores were prepared from carboxyl-terminated PLGA, and the positively charged cores were prepared by modifying carboxyl-terminated PLGA particles with polyethyleneimine (PEI). Upon mixing PLGA-COOH cores with 5% PEI solution, a change in surface

charge from -45 mV to +27 mV was observed with negligible effect on the nanoparticle size (ESI Fig. S5†). The two oppositely charged cores were then used to prepare RBC-NPs using the extrusion method.

Unlike the negatively charged cores, which were readily extruded with RBC membrane vesicles to form RBC-NPs, the positively charged cores formed observable aggregates upon mixture with the vesicles. Extruding the positively charged cores with RBC membrane vesicles through 200, 400, and 1000 nm porous polycarbonate membranes resulted in significant membrane clogging that impeded the extrusion process. To better examine the membrane/particle interactions, the particle/membrane mixtures were visualized using transmission electron microscopy (TEM). The negatively charged cores formed consistent spherical particles with a core-shell structure (Fig. 4A). The absence of aggregates in membranes mixed with negatively charged cores suggests a more subtle membrane/particle interaction that is less disruptive to membrane structure and fluidity (Fig. 4B). In contrast, the positively charged cores coalesced into large polydisperse aggregates with the membranes (Fig. 4C). The aggregate formation can likely be attributed to the strong electrostatic interactions between positively charged cores and the negatively charged RBC membranes. Owing to the dense, negatively charged sialyl moieties on the extracellular membrane side, the strong affinity to positively charged nanoparticles could collapse the fluidic lipid bilayer and impede the local arrangement necessary for lipid coverage.[30] Bridging between cores and collapsed lipid membranes with opposite charges can therefore account for the observed aggregate formation (Fig. 4D). While understanding the dynamics between the negatively charged cores and RBC membranes demands in-depth molecular analysis beyond the scope of the

present study, we demonstrate that the negative surface charge is a major factor in enabling proper RBC-NP formation. The electrostatic repulsion between negatively charged particle surfaces and asymmetrically charged RBC membranes also provides a driving force that favors the right-side-out membrane orientation on the RBC-NPs.

2.3.5 Surface Curvature of Polymeric Cores Affecting RBC Membrane Coating

As lipid bilayer coating on nanoscale substrates can be influenced by the substrates' radius of curvature,[31] or, alternatively speaking, the cores' size, we demonstrate the applicability of the RBC membrane cloaking process over a range of particle sizes that are relevant for nanomedicine applications. We prepared carboxyl-terminated PLGA cores of different diameters using variations of the solvent displacement method,[32] creating unimodal nanoparticles that ranged from 65 nm to 340 nm. Each of these PLGA nanoparticle cores was extruded with corresponding amount of RBC membrane vesicles (ESI) through polycarbonate membrane with appropriate pore sizes to form RBC-NPs. For all the differently sized particles, RBC membrane coating resulted in an increase in size by 10 ~ 20 nm. The cloaking process also shifted the zeta potential of the particles from approximately -45 mV to -24 mV, which corresponds closely to the zeta potential of RBC membrane vesicles (Fig. 5A and ESI Fig. S6†). TEM visualization of particle cores 65, 120, 200, and 340 nm in diameter showed that uniform RBC membrane cloaks were broadly applied (Fig. 5B). The flexibility of the membrane coating technique offers the freedom to functionalize a broad range of nanodevices with different sizes and geometries. The size of RBC-NPs can also be fine-tuned to match the need of specific medical applications.

2.4 Discussion

By examining multiple interfacial aspects of RBC-NPs, the present study provides a better understanding of the platform. The particles were shown to be completely enveloped, suggesting a continuous membrane coating on the particle surfaces. The completeness of membrane coverage has significant implications as it can shield the particles from external exposure, thereby minimizing the risk of complement activation and immunological responses typically associated with foreign materials. The RBC-NPs were also found to possess right-side-out oriented membrane coating, which exposes dense surface glycan contents to the aqueous environment and ensures the proper protein presentation on the particle surface.[10] The hydrophilic glycan layer also enhances the colloidal stability of RBC-NPs under ionic conditions, and its enzymatic removal by trypsin led to rapid particle aggregation. Taken together with previous findings that demonstrate the membrane and surface protein retention[6] and cargo encapsulation by the particles,[33] the RBC-NPs can be considered a multifunctional nanoparticle system that integrates the steric stabilization of polysaccharides, the biological immunoevasive activities of membrane proteins, the cargo loading capacity of polymeric cores, and the anchoring and insulating functions of the lipid membranes, into a single, unified package. The present study also demonstrates RBC-NPs' size-tunability and enzyme-triggered particle destabilization. These features provide the platform with the opportunity to be tailored for specific delivery goals.

In addition to elucidating structural composition of RBC-NPs, the present study also extends the understanding of cell membrane/nanoparticle interaction that drives the membrane cloaking process. Both the surface glycans on RBC membranes and the

physicochemical properties of nanoparticle cores were found to play significant roles in RBC-NP formation. With carboxy-terminated PLGA cores as nanoparticle substrates, the membrane cloaking process was highly efficient. Achieving complete particle shielding and particle stabilization requires a membrane-to-polymer ratio closely matched to the theoretical value for complete particle coverage. This efficient cloaking process can be attributed to the glycan-driven colloidal stabilization of the polymeric particles, which renders the system energetically favorable. The asymmetrically distributed sialic acids, which bestow a negative charge to the extracellular membrane side, can also affect membrane-particle interaction electrostatically. Rapid aggregation occurred upon the mixture of positively charged polymeric cores with RBC membranes, as strong electrostatic attractions resulted in membrane-particle bridging. In contrast, negatively charged cores readily form RBC-NPs with right-side-out membrane coating, which is likely aided by the repulsion between particle and extracellular membrane surfaces. As surface sialic acids and their associated membrane charge asymmetry are broadly present in biology,[34,35] such membrane-particle interaction should be considered broadly in the development of cell membrane-functionalized nanodevices.

2.5 Conclusions

RBC-NPs present a unique nanocarrier platform that combines the immunomodulatory properties of natural cellular components with the cargo carrying capacity of polymeric nanoparticles. In the present study, we examined the platform's interfacial features and assessed the roles of RBC surface glycans and nanoparticle properties in RBC-NP formation. RBC-NPs are completely shielded by lipid membranes and are stabilized by surface glycans. The hydrophilic glycans and the negatively charged

sialic acid residues contribute to the structural organization of RBC-NPs, which possess a unilamellar, right-side-out membrane cloak. Owing to the inherent electrostatic properties of RBC membranes, positively charged nanoparticles did not yield proper RBC-NP formation. The membrane cloaking approach was successfully applied to nanoparticle substrates between 65 and 340 nm in diameter, demonstrating the versatility of the camouflaging technique toward a variety of nanocarriers.

Chapter 2, in full, is a reprint of the material as it appears in Nanoscale 2014. Luk, B.; Hu, C-M.; Fang, R.; Dehaini, D.; Carpenter, C.; Gao, W.; Zhang, L. are the co-authors of this material.

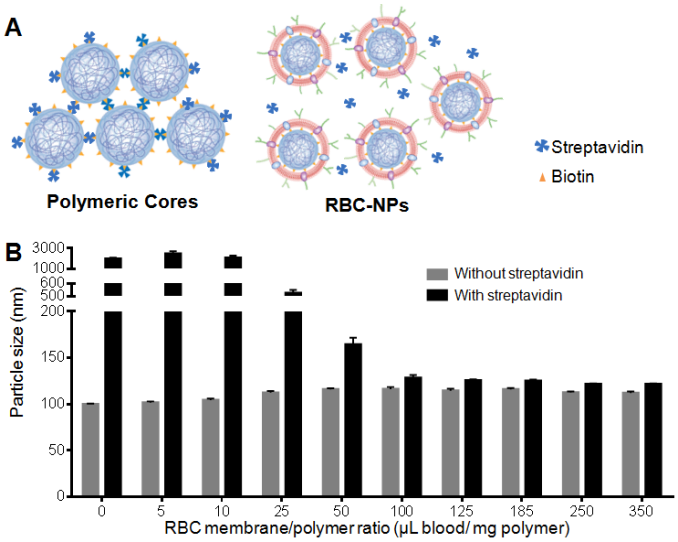

Figure 2.1. Determination of the completeness of RBC membrane coating. (A) Schematic illustration shows the membrane coverage assay in which RBC membrane coating precludes the binding of free streptavidin to the biotin immobilized on the surface of polymeric cores. (B) Size change of RBC-NPs due to streptavidin/biotin cross-linking at various RBC membrane-to-polymer ratios. Error bars represent standard deviation (n =3).

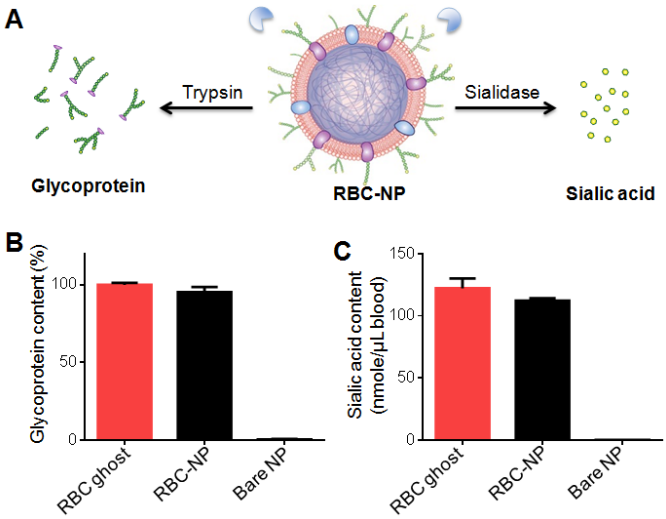

Figure 2.2. Quantification of glycoprotein and sialic acid on RBC-NPs to examine the sidedness of RBC membranes. (A) Schematic demonstrating the use of trypsin and sialidase to remove exoplasmic glycoprotein and sialic acid from RBC-NPs, respectively. (B) Comparison of the relative glycoprotein content recovered from equivalent amount of RBC ghosts, RBC-NPs, and bare NPs after trypsinization (n = 3). (C) Comparison of the sialic acid content recovered from equivalent amount of RBC ghosts, RBC-NPs, and bare NPs after sialidase treatment (n = 3).

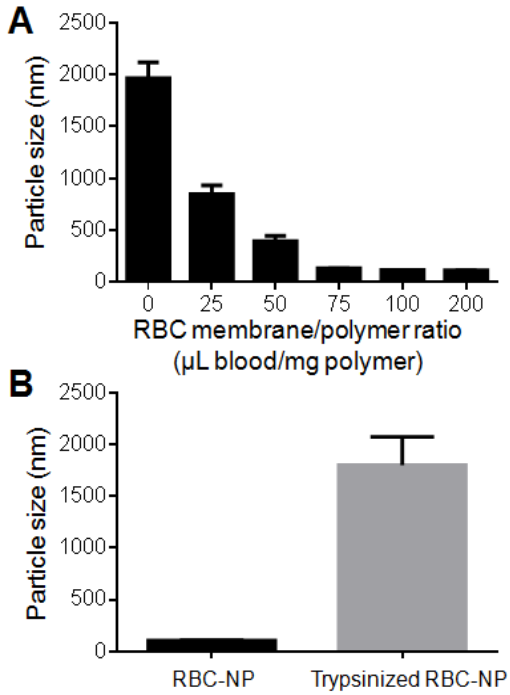

Figure 2.3. Stabilization of polymeric cores by RBC membrane cloaking. (A) Size of RBC-NPs prepared from different RBC membrane-to-polymer ratios. For given amount of polymeric particles, the particles become more stable in PBS buffer with increasing RBC membrane content. Error bars represent standard deviation (n = 3). (B) Sizes of stable RBC-NPs before and after trypsinization. Trypsinization resulted in the loss of particle stability (n = 3).

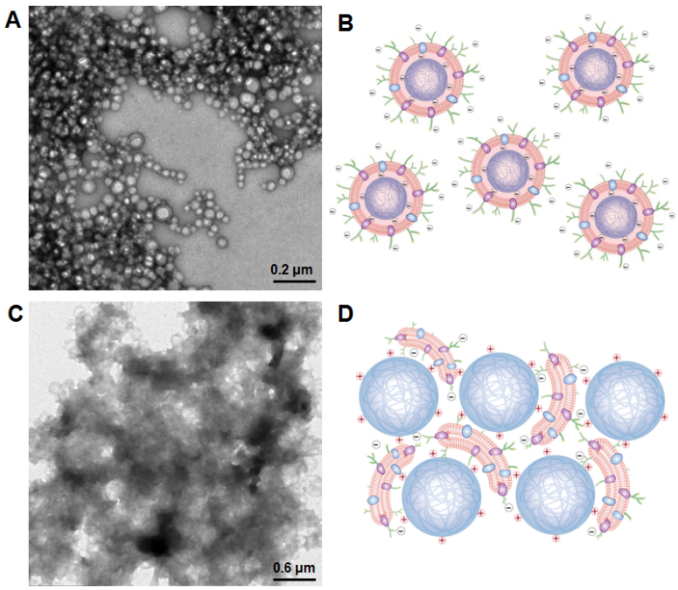

Figure 2.4. Effect of particles' surface charge on RBC membrane coating. (A) Representative transmission electron microscopy (TEM) image of negatively charged polymeric particles extruded with RBC membranes. (B) Schematic conceptualization of the electrostatic interaction between negatively and asymmetrically charged RBC membrane with negatively charged polymeric cores. (C) Representative TEM image of positively charged polymeric cores extruded with RBC membranes. (D) Schematic conceptualization of the electrostatic interaction between negatively and asymmetrically charged RBC membrane with positively charged polymeric cores.

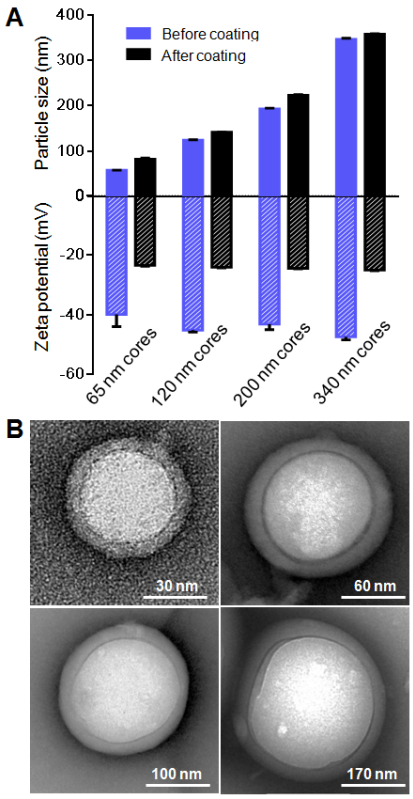

Figure 2.5. Effect of particles' surface curvature on RBC membrane coating. (A) Size and surface zeta potential of RBC-NPs with differently sized, negatively charged polymeric cores, both before and after RBC membrane coating. (B) Representative TEM images of RBC-NPs with differently sized polymeric cores.

2.6 References

1 J. Yoo, D. Irvine, D. Discher, S. Mitragotri, *Nat. Rev. Drug Discovery*, 2011, 10, 521.

2 S. Balmert, S. Little, *Adv. Mater.,* 2012, 24, 3757.

3 C. Hu, R. Fang, B. Luk, L. Zhang, *Nanoscale*, 2013, DOI: 10.1039/c3nr05444f.

4 R. Tsai, P. Rodriguez, D. Discher, *Blood Cells, Mol. Dis*., 2010, 45, 67.

5 P. Rodriguez, T. Harada, D. Christian, D. Pantano, R. Tsai, D. Discher, *Science*, 2013, 339, 971.

6 C. Hu, L. Zhang, S. Aryal, C. Cheung, R. Fang, *Proc. Natl. Acad. Sci. U.S.A.*, 2011, 108, 10985.

7 W. Gao, C. Hu, R. Fang, B. Luk, J. Su, L. Zhang, *Adv. Mater.,* 2013, 25, 3549.

8 C. Hu, R Fang, J. Copp, B. Luk, L. Zhang, *Nat. Nanotechnol,* 2013, 8, 336.

9 R. Fang, C. Hu, K. Chen, B. Luk, C. Carpenter, W. Gao, S. Li, D. Zhang, W. Lu, L. Zhang, *Nanoscale*, 2013, 5, 8884.

10 C. Hu, R. Fang, B. Luk, K. Chen, C. Carpenter, W. Gao, S. Li, D. Zhang, W. Lu, L. Zhang, *Nanoscale*, 2013, 5, 2664.

11 N. Doshi, S. Zahr, S. Bhaskar, J. Lahann, S. Mitragotri, *Proc. Natl. Acad. Sci. U.S.A.,* 2009, 106, 21495.

12 T. Merkel, S. Jones, K. Herlihy, F. Kersey, A. Shields, M. Napier, J. Luft, H. Wu, W. Zamboni, A. Wang, J. Bear, J. DeSimone, *Proc. Natl. Acad. Sci. U.S.A.*, 2011, 108, 586.

13 C. Hu, R. Fang, L. Zhang, *Adv. Healthcare Mater*., 2012, 1, 537.

14 M. Mager, V. LaPointe, M. Stevens. *Nat. Chem.*, 2011, 3, 582.

15 W. Evans, J. Graham, *Membrane Structure and Function*, Oxford Univ. Press, New York, 1991, pp. 1-86.

16 E. Eylar, M. Madoff, O. Brody, J. Oncley, *J. Biol. Chem.*, 1962, 237, 1992.

17 M. Fukuda., *Molecular Glycobiology*, Oxford Univ. Press, New York, 1994, pp. 1-52.

18 R. Schauer, *Curr. Opin. Struct. Biol.*, 2009, 19, 507.

19 S. Kelm, R. Schauer, *Int. Rev. Cytol.,* 1997, 175, 137.

20 P. Raveendran, J. Fu, S. Wallen, *J. Am. Chem. Soc.*, 2003, 125, 13940.

21 C. Cho, J. Jeong, T. Ishihara, R. Takei, J. Park, K. Park, A. Maruyama, T. Akaike, *Biomaterials,* 1997, **18**, 323.

22 C. Lemarchand, R. Gref, P. Couvreur, *Eur. J. Pharm. Biopharm.,* 2004, **58**, 327.

23 J. Rothman, J. Lenard, *Science*, 1977, **195**, 743.

24 T. Steck, G. Dawson, *J. Biol. Chem.*., 1974, **249**, 2135.

25 R. Winzler, *Red Cell Membrane*, Lippincott, Philadelphia, 1969, pp. 157.

26 H. Heidrich, G. Leutner, *Eur. J. Biochem,* 1974, **41**, 37.

27 A. Miller, J. Sullivan, J. Katz, *Cancer Res.,* 1963, **23**, 485.

28 J. Durocher, R. Payne, M. Conrad, *Blood*, 1975, **45**, 11.

29 S. Mornet, O. Lambert, E. Duguet, A. Brisson, *Nano Lett.*, 2005, **5**, 281.

30 M. Fischlechner, M. Zaulig, S. Meyer, I. Estrela-Lopis, L. Cuellar, J. Irigoyen, P. Pescador, M. Brumen, P. Messner, S. Moya, E. Donath, *Soft Matter,* 2008, **4**, 2245.

31 Y. Roiter, M. Ornatska, A. Rammohan, J. Balakrishnan, D. Heine, S. Minko, *Nano Lett.,* 2008, **8**, 941.

32 J. Chan, L. Zhang, K. Yuet, G. Liao, J. Rhee, R. Langer, O. Farokhzad, *Biomaterials,* 2009, **30**, 1627.

33 S. Aryal, C. Hu, R. Fang, D. Dehaini, C. Carpenter, D. Zhang, L. Zhang, *Nanomedicine (London, U.K.)*, 2013, **8**, 1271.

34 R. Schauer, *Adv. Carbohydr. Chem. Biochem.*, 1982, **40**, 131.

35 M. Glick, C. Comstock, M. Cohen, L. Warren, *Biochim. Biophys. Acta*, 1971, **233**, 247.

3 Erythrocyte Membrane-Cloaked Polymeric Nanoparticles for Controlled Drug Loading and Release

*Nanomedicine 2013

3.1 Introduction

In the past decades, advances in engineering materials at the nanometer scale have resulted in a myriad of nanoparticle (NP)-based drug delivery systems in clinical applications.[1, 2] The unique advantages of these nanomedicines, particularly their improvement on existing therapeutic agents through altered pharmacokinetics and biodistribution profiles, hinge on their ability to circulate in the blood stream for a prolonged period of time.[3, 4] As a result, considerable research interest has been focused on the search of novel materials, both naturally and synthetically made, that allow NPs to bypass macrophage uptake and systemic clearance.[5, 6] Meanwhile, strategies aimed at extending particle residence time *in vivo* through modifying NP physicochemical properties including size, shape, deformity, and surface characteristics have also been extensively explored.[7, 8]

In this perspective, we recently developed a red blood cell membrane (RBCm)-cloaked NP drug delivery system with combined advantages of a long circulation lifetime from RBCs and controlled drug retention and releases from polymeric particles.[9] Our top-down approach, based on the extrusion of polymeric particles mixed with preformed RBCm-derived vesicles, translocated the entire RBCm with preserved membrane proteins to the surface of sub-100-nm polymeric cores, resulting in NPs cloaked by the erythrocyte exterior for long systemic circulation. This cell-mimicking strategy provides

a cellular membrane medium surrounding polymeric cores for transmembrane protein anchorage, hence avoiding chemical modifications in conventional NP surface fictionalizations that could compromise the integrity and functionalities of the proteins.

In our continuing efforts to further develop this cell-mimicking NP platform for advanced drug delivery applications, herein, we report formulation strategies of loading small-molecule chemotherapy drugs such as doxorubicin (DOX), a model anti-cancer drug, into the NPs and study drug release kinetics with an emphasis on the role played by RBCm cloak in drug retention. Specifically, to load DOX molecules into NP core, we explored two distinct strategies: physically encapsulating drug molecules into the polymer matrix and chemically conjugating drug molecules to the polymer backbones, and showed that they resulted in distinct drug loading yields and release kinetics. We further formulated NPs with the same polymer cores as RBCm-cloaked NPs, but coated by poly (ethylene glycol) (PEG, PEGylated NPs) rather than RBCm. Comparison of drug release profiles of the two delivery systems demonstrated that RBCm cloak provides a barrier retarding the outward diffusion of encapsulated drug molecules, and therefore can be potentially exploited to better control drug releases. Additionally, in an attempt to examine the therapeutic potential of the RBCm-cloaked NPs, we chose an acute myeloid leukemia (AML) Kasumi-1 cell line and showed that DOX-loaded RBCm-cloaked NPs exhibited higher toxicity in comparison to the same amount of free DOX.

3.2 Materials and Methods

3.2.1 RBC ghost derivation

RBC ghosts devoid of cytoplasmic contents were prepared following previously published protocols.[9, 10] Briefly, whole blood, withdrawn from male ICR mice (6–8

weeks, Charles River Laboratories) through cardiac puncture with a syringe containing a drop of heparin solution (Cole-Parmer), was centrifuged (800 × g for 5 min at 4 °C) to remove serum and buffy coat. The packed RBCs were washed in ice cold 1× PBS, treated by hypotonic medium for hemolysis, and then suspended in 0.25× PBS in an ice bath for 20 min. The hemoglobin was removed by centrifuging the suspension at 800 ×g for 5 min. RBC ghosts in the form of a pink pellet were collected.

Preparation of RBCm-derived vesicles

The collected RBC ghosts were sonicated in a capped glass vial for 5 min using a FS30D bath sonicator (Fisher Scientific) at a frequency of 42 kHz and power of 100 W. The resulting vesicles were subsequently extruded repeatedly through 400 nm and then 200 nm polycarbonate porous membranes by using an Avanti mini extruder (Avanti Polar Lipids). After each extrusion, the size of the RBCm-derived vesicles was monitored by dynamic light scattering (DLS, Nano-ZS, model ZEN3600).

3.2.2 Ring-opening polymerization of L-lactide

DOX-poly(lactide acid) (PLA) conjugates were synthesized based on a published protocol.[11, 12] Briefly, ring-opening polymerization of L-lactide (Sigma-Aldrich, USA) was catalyzed by an alkoxy complex (BDI)ZnN($SiMe_3$)$_2$ in a glove-box filled with argon at room temperature. (BDI)ZnN($SiMe_3$)$_2$ (6.4 mg, 0.01 mmol) and DOX (Jinan Wedo Co., Ltd., Jinan, China) (5.4 mg, 0.01 mmol) were mixed in anhydrous tetrahydrofuran (THF, 0.5 mL), where L-lactide (101 mg, 0.7 mmol) dissolved in 2 mL of anhydrous THF was added dropwise. After the L-lactide was completely consumed as indicated by ^{1}H NMR (Varian Mercury 400 MHz spectrometer), the crude product was precipitated in cold diethyl ether and purified by multiple dissolution-precipitation cycles. The

conjugation was confirmed by ^{1}H NMR and conjugates had a molecular weight of ~10,000 g/mol determined by gel permeation chromatography (GPC, Viscotek, USA).

3.2.3 Preparation of NP core and loading of DOX

The DOX-PLA conjugate was first dissolved in acetonitrile to form 1 mg/mL solution and 1mL of such solution was added dropwise to 3mL of water. The mixture was then stirred in open air for 2 hours, allowing acetonitrile to evaporate. The resulting solution of NP cores was washed by Amicon Ultra-4 Centrifugal Filters (Millipore, 10 kDa cut-off) to completely remove organic solvent residues. The particles were then re-suspended in 1 mL distilled water. To physically encapsulate DOX, 1 mg poly(lactic-co-glycolic acid) (PLGA, 0.67 dL/g, carboxy-terminated, LACTEL Absorbable Polymers) was first dissolved into 1 mL acetonitrile, followed by the addition of DOX pre-dissolved in 25 μL of dimethyl sulfoxide (DMSO). Similar procedures as described above were followed to generate suspensions containing NP cores.

3.2.4 Fusion of RBCm-derived vesicles with NP cores

To fuse the RBCm-derived vesicles with the aforementioned NP cores, suspensions containing 1 mg of NP cores was first mixed with RBCm-derived vesicles prepared from 1 mL of whole blood. The mixture was then extruded 11 times through a 100-nm polycarbonate porous membrane with an Avanti mini extruder. To fully coat 1 mg of NP cores, an excess of blood was used to compensate for the membrane loss during RBC ghost derivation and extrusion.[9]

3.2.5 Preparation of PEGylated NPs

The DOX-PLA conjugate and PLA-PEG-COOH (M_w = 10 kDa, PDI = 1.12; PEG = 3.5 kDa, PLA = 6.5 kDa)[13] at a weight ration of 1:1 was first dissolved in acetonitrile at

a concentration of 1 mg/mL, followed by the same procedures as described above to produce NP suspensions. To physically encapsulate DOX into PEGylated NPs, 1 mg poly(lactic-co-glycolic acid) (PLGA, 0.67 dL/g, M_w = 40 kDa, carboxy-terminated, LACTEL Absorbable Polymers) was first dissolved into 1 mL acetonitrile, followed by the addition of 100 μg DOX dissolved in 25 μL of DMSO. Same procedures as described above were used to produce NP suspensions.

3.2.6 NP stability studies

NP stability in PBS was assessed by monitoring particle size using DLS. Specifically, 500 μg NPs were suspended in 1 mL 1× PBS and the sizes were measured in triplicate at room temperature every 24 hours over a period of one week. Between measurements, samples were incubated at 37 °C with gentle shaking. NP serum stability was evaluated by monitoring the UV-absorbance at the wavelength of 560 nm. Specifically, NPs were first concentrated to 2 mg/mL in PBS, followed by the addition of 2× fetal bovine serum (FBS, Hyclone) of equal volume. The absorbance was measured by using an Infinite M200 multiplate reader at 37 °C approximately every 1 minute over a period of 2 hours. The morphology and particle size were further characterized using scanning electron microscopy (SEM). Samples for SEM were prepared by dropping 5 μL of NPs solutions onto a polished silicon wafer. After drying the droplet at room temperature overnight, the sample was coated with chromium and then imaged by SEM.

3.2.7 Measurement of drug loading yield and releases

The concentration of DOX in a solution was determined by measuring florescence intensities at 580 nm with excitation wavelength of 480 nm. To determine DOX loading yield of NPs, the above fluorescent measurement was carried out after incubating 100 μL

NP solution with 100 μL 0.1 M HCl in acetonitrile for 24 hours, all fluorescent measurements were performed at the same condition with 0.1 M HCl. To plot DOX release profiles, 200 μL NP solution (1 mg/mL) was loaded into a Slide-A-Lyzer MINI dialysis microtube (Pierce, Rockford, IL, molecular weight cutoff = 3.5 kDa) and then dialyzed against 2 L of PBS (pH = 7.4) at 37 ^{o}C. PBS buffer was changed every 12 hours during the whole dialysis process. At each predetermined time point, NP solutions from three mini dialysis units were collected and DOX concentration was measured. Note that the hydrophobic DOX-PLA conjugates are unlikely to be released from the hydrophobic particles to aqueous solutions, because that is an energetically unfavorable process. It is expected that only the drug molecules detached from the polymer chains will be released.

3.2.8 Cell viability assay

Cytotoxicity of free DOX and DOX-loaded NPs was assessed against Kasumi-1 cell line established from the peripheral blood of an acute myeloid leukemia (AML) patient using MTT assay (Promega Corporation, Madison,WI, USA). Cells were first seeded (~ 5×10^3 per well) in 96-well plates and then incubated for 24 hours. After the addition of free DOX or DOX-loaded NPs, the cells were incubated for additional 72 hours. Cell viability was then determined by using MTT assay following a protocol provided by the manufacturer.

Results and Discussion

3.2.9 Preparation of RBCm-cloaked NPs

The preparation process of RBCm-cloaked NPs was based on our previously published protocol and schematically illustrated in Fig. 1.[9] Briefly, purified RBCs first underwent membrane rupture in a hypotonic environment to remove its intracellular

contents. Next, the emptied RBCs (~2 μm in diameter) were washed and extruded through 100-nm porous membranes to create RBC-membrane derived vesicles (~200 nm in diameter). Meanwhile, polymeric cores (~70 nm in diameter), such as those made from PLA or PLGA, were prepared by using a solvent displacement method. The resulting polymeric cores were subsequently mixed with RBC-membrane derived vesicles and the mixture was physically extruded through 100-nm pores, where the two components fused under the mechanical force and formed RBCm-cloaked NPs (~90 nm in diameter).

3.2.10 Loading of doxorubicin (DOX) into RBCm-cloaked NPs

In this study, we examined two distinct methods to load DOX as a model drug into the RBCm-cloaked NPs: physical encapsulation and chemical conjugation. Physical encapsulation is achieved by first mixing DOX and polymers in acetonitrile, followed by precipitation into water. In this case, drug loading yield can be varied through different formulation parameters. For example, when varying initial DOX to PLGA weight ratio from 5 % to 20 %, the loading yield increased from 0.9 % to 1.8 % (see Fig. 2).

Alternatively, DOX molecules can be loaded into NP cores by covalently conjugating drug molecules to polymer backbones. Intuitively, DOX molecules can be directly conjugated to carboxyl terminated PLA chains through hydroxyl groups; however, this approach causes heterogeneities for polymer-drug conjugates, owing largely to the polydispersity of the polymer chains, the lack of control over the regio- and chemoselective conjugation of the DOX molecules containing multiple hydroxyl groups, and the lack of control over the conjugation efficiency. Therefore, we adopted an alternative approach, where the hydroxyl group of the DOX, with the presence of L-lactide monomer and (BDI)ZnN($SiMe_3$)$_2$ as a catalyst, were utilized to initiate the ring

opening polymerization (ROP) and led to the formation of PLA-DOX conjugates.[11, 12] In this approach, as the polymerization reaction is initiated by the drug molecule itself, a conjugation efficiency of near 100% can be achieved. In addition, the metal amido catalyst (BDI)ZnN($SiMe_3$)$_2$ preferentially allows for PLA propagation at C_{14}-OH position of DOX instead of its more sterically hindered C_4'- and C_9-OH positions. After the reaction was terminated, products were purified by using repeated dissolution-precipitation cycles and then characterized by using ^{1}H-NMR spectroscopy. Proton resonance peaks corresponding to both DOX molecules and PLA backbones are present, including the aromatic protons of DOX between δ = 7.5 and 8.0 ppm, protons of -CH_3 group of PLA at δ = 1.5 ppm, and -CH group of PLA at δ = 5.2 ppm, hence confirming the formation of PLA-DOX conjugates [11]. In contrast to physical encapsulation, where the drug loading yield primarily depends on formulation parameters, in chemical conjugation, drug loading yield is dictated by polymer chain length, which is in turn determined by polymerization conditions such as initiator (DOX)-to-monomer ratio. For example, the PLA-DOX conjugates synthesized in our study were found to have a molecular weight of 10 kDa and a narrow polydispersity index (PDI) of 1.16, corresponding to an approximately 5% loading yield of DOX after the conjugates were formulated into the NPs (see Fig. 2).

3.2.11 In vitro stability of DOX-loaded RBCm-cloaked NPs

Next, we studied the stability of DOX-loaded RBCm-cloaked NPs in physiologically relevant buffer solutions. In PBS, NP stability is monitored by measuring NP sizes at different time points, as unstable particles tend to aggregate and their sizes increase. In our study (Fig. 3A), NPs loaded with DOX molecules by using both physical

encapsulation and chemical conjugation showed similar initial diameters of ~ 90 nm without significant size increase over the span of one week. Similarly, only a slight change in the PDIs of the NPs was observed over the same time span, indicating a high stability of DOX-loaded RBCm-cloaked NPs in PBS. NP stability was further examined in serum by monitoring UV absorbance at 560 nm, a characteristic wavelength reflecting the extent of particle aggregation.[14, 15] RBCm-cloaked NPs, loaded with DOX molecules by either physical encapsulation or chemical conjugation, showed a nearly constant absorbance at 560 nm over a time span of two hours (Fig. 3B), suggesting that the NPs are highly stable in 100% fetal bovine serum (FBS). The morphological measurements of these RBCm-cloaked NPs by SEM showed spherical structures with an average size of about 75 nm (Fig 3C). In contrast, absorbance of bare polymeric cores made from PLGA or PLA-DOX conjugates without RBCm cloaks immediately increased upon addition into FBS, thus we were unable to monitor their long-term stability in either PBS or serum. Our results showed that the RBCm cloak played a significant role in stabilizing NPs in both buffer solutions and serum. From a practical perspective, the fast aggregation of uncoated polymeric particles in buffer solutions provided a way of selective precipitation and removal of uncoated particles from RBCm-cloaked NPs after their preparation.

3.2.12 Release kinetics of DOX from RBCm-cloaked NPs

Following the formulation of stable DOX-loaded RBCm-cloaked NPs, we proceeded to investigate their DOX release kinetics (Fig. 4). We first examined how different drug loading mechanisms would affect DOX releases from RBCm-cloaked NPs. Our results showed that, when DOX molecules were physically encapsulated into the polymer matrix, the drug release rate was significantly faster, as 20% of DOX molecules

were released within the first two hours from the RBCm-cloaked NPs. In contrast, when formulations of chemical conjugation were examined, within the first two hours, only 5% of DOX molecules were released. Such difference has been attributed to the fact that covalent bonding of DOX molecules to the polymer backbone requires drug molecules first be hydrolyzed from the polymer by bulk erosion before they can diffuse out of the polymeric matrix for release.[11, 12, 16] A more sustained release profile resulted from drug-polymer covalent conjugation also suggests that chemical linkers responsive to environmental triggers can achieve better-controlled drug releases when developing RBCm-cloaked NPs for advanced drug delivery applications.[13, 17] It is expected that acidic pH conditions will increase the drug release rate of the polymeric cores because the pH drop will accelerate the degradation rate of the polymer backbone and facilitate the cleavage of the ester linkage between the drugs and the polymers as well.[11]

In order to gain a better understanding on the role played by RBCm cloak in drug retention, we followed an established procedure to generate NPs by blending PLA-PEG di-block copolymers and resulted in PEGylated NPs, where NP cores were coated and stabilized by a surrounding PEG layer instead of RBCm cloak.[18] We hypothesize that if two formulations have similar NP cores, the difference in drug releases will be primarily caused by the different abilities of RBCm cloak and surface PEG coating in drug retention. By comparing DOX release from RBCm-cloaked NPs to that from PEGylated NPs, we found that the release rate of the RBCm-cloaked NPs was lower: approximately 20% of DOX was released within of the first 72 hours in the RBCm-cloaked NPs, whereas 40% of DOX was released from the PEGylated NPs over the same time span. In fact, by using NPs formulated by PLGA-PEG di-block copolymers, surface PEG

molecules have been found to hinder drug release from NP cores.[19] Hence, our observation, where DOX is released at a higher rate from PEG-coated NPs compared to RBCm-cloaked NPs, indicates that RBCm indeed acts as a diffusion barrier for DOX release. This observation also in accordance with previous studies showing that phospholipid coating can act as a barrier to drug diffusion [20]. Such a role played by RBCm cloak further suggests that strategies aimed at engineering lipid membrane coatings may allow for responsive drug releases from RBCm-cloaked NPs under certain environmental cues in addition to those achieved by chemical conjugations embedded in polymer cores.[21]

To gain a quantitative understanding on the membrane coating effect on drug retention, the drug release profiles were analyzed using mathematic models established in pervious particle drug release studies. Since the degradation of PLGA is on the order of weeks,[22, 23] markedly slower than the observed drug release for the physically loaded systems, a diffusion-dominant Higuchi model was applied to both RBCm-coated and PEGylated NPs containing physically encapsulated DOX. Plotting the drug release percentage against the square root of time yielded linear fittings with R^2=0.98 and 0.96 for the RBCm-cloaked and the PEGylated NPs, respectively (Fig. 4B). The goodness of the fit implies a diffusion-controlled drug release mechanism and further allows for the derivation of the diffusion coefficient through the following Higuchi equations:[24, 25]

$$M_t = Kt^{1/2} \qquad (1)$$

$$K = A(2C_{ini}DC_s)^{1/2} \qquad (2)$$

where, M_t is drug release at time t in hours, K is the Higuchi constant, C_{ini} is the initial drug concentration, C_s is the drug solubility, A is the total surface area of the particles,

and *D* is the diffusion coefficient. Given the particle dimensions, the drug loading yield, the solubility of DOX in water (1.18 g/L), and the drug release data, the diffusion coefficients were determined to be 6.6×10^{-16} cm^2/sec and 8.2×10^{-16} cm^2/sec for the RBCm-clocked and PEGylated NPs, respectively, which are also consistent with previously reported drug diffusivities from PLGA/PLA NPs.[26] In our study, the bilayered membrane coating reduced the drug diffusivity by 1.2 times. We expect this retardation effect by the RBCm cloak would likely vary with different particle sizes, polymer types, and therapeutic cargoes.

On the other hand, applying zero order, first order, and Higuchi models to the drug release profiles of chemically conjugated DOX yielded poor fittings (data not shown), indicating complex release kinetics when additional drug cleavage is coupled with drug diffusion out of the polymer matrix. Precise modeling of retardation effect imposed by the RBCm cloak on the chemically conjugated DOX is beyond the scope of this study. Nevertheless, as identical particle cores are present in both RBCm-cloaked and PEGylated NPs, herein, we hypothesize that polymer matrix relaxation and hydrolytic cleavage of the linkage are not dominant factors contributing to the difference observed in DOX release profiles. Instead, we contribute the slower release rate of the RBCm-cloaked NPs to two diffusion-dominated components: the diffusion of water into the polymer matrix and the diffusion of the cleaved drugs outward across the polymer matrix.[27] As the membrane coating was shown to decrease the drug diffusivity in the physical entrapment system, it likely affected both the influx of water and the efflux of cleaved drugs in the covalent conjugate system, thereby resulting in a more sustained drug release profile.

3.2.13 Cytotoxicity of DOX-loaded RBCm-cloaked NPs

Lastly, we examined the therapeutic potential of the DOX-loaded RBCm-cloaked NPs against an AML Kasumi-1 cell line. AML, an illness characterized by uncontrolled growth and accumulation of leukemia blasts in the blood stream, was chosen as a disease target because of the RBCm-cloaked NPs' long circulation lifetime in the blood stream and their sustained drug release profiles. The current standard of care for AML is high-dose anthracyclines, which raises serious concerns for cardiac toxicity.[28] Long-circulating NPs releasing therapeutic compounds in a sustained manner offer the opportunity to reduce the necessary dosing and improve on the treatment efficacy. RBCm-cloaked NPs, where DOX were either physically loaded or covalently conjugated, exhibited higher toxicity in comparison to free DOX over a 72-hour incubation period (Fig. 5). In a previous study, we have demonstrated that these RBCm-cloaked NPs can be taken up by cancer cells in a tissue culture and the NPs remain an intact core-shell structure after cellular internalization.[9] So the observed enhancement in efficacy can be likely attributed to endocytic uptake of NPs, which enables a high payload of drugs to enter the intracellular region.[29] Several previous reports have shown enhanced cytotoxicity of DOX through NP-based delivery of DOX.[30, 31] The free DOX, in contrast, relies on passive membrane diffusion for cellular entry, which is less efficient and susceptible to membrane-bound drug efflux pumps.[32-34] AML cells, including Kasumi-1 cell line, are known to express membrane-bound drug efflux pumps, which decrease intracellular compartmentalization of DOX.[35] Our study suggests that RBCm-cloaked NPs, with a prolonged circulation lifetime, sustained drug release, and improved cell internalization,

can become a promising platform toward the treatment of blood cancer. Further studies are warranted to investigate the therapeutic potential of these NPs *in vivo*.

3.3 Conclusions

In summary, herein, we examined two strategies for loading drugs into an RBCm-cloaked NP delivery system: physical encapsulation and chemical conjugation. Release studies suggested that chemical conjugation strategy resulted in a more sustained drug release profile. We further formulated PEGylated NPs that had the same NP cores but different surface coatings compared to RBCm-cloaked NPs. By comparing drug release profiles of these two delivery systems, we demonstrated that RBCm cloak provided a barrier slowing down the outward diffusion of encapsulated drug molecules. Our results suggest that chemical modifications on drug-polymer linkage in the NP core and engineering on the NP surface coatings can be both explored to gain better controls over drug releases of RBCm-cloaked NPs. In a following efficacy study by using AML Kasumi-1 cell line, RBCm-cloaked NPs exhibited higher toxicity in comparison to free DOX. The previously observed long systemic circulation lifetime in the blood stream and the sustained drug release kinetics reported hereby indicate that this biomimetic drug delivery system may hold great promise for systemic delivery of payloads for the treatment of various diseases such as blood cancers. With further development, these RBCm-cloaked NPs are expected to become a robust drug delivery system that combines the advantages of both synthetic polymers and natural cellular membranes.

3.4 Future Perspective

RBCm-cloaked NPs represent a novel class of NP formulations bringing together both the long circulation lifetime of RBC and controlled drug retention and releases of synthetic polymers. After gaining a deeper understanding on the roles played by the RBCm shell and the polymeric core, this NP formulation can be further tailored by engineering both parts to improve systemic delivery of therapeutic payloads. We believe that with continuing effort, this formulation will result in a robust delivery platform and make significant impacts on both biomedical applications and nanotechnology research.

3.5 Executive Summary

- *NP Preparation:* To combine the advantages of a long circulation lifetime from RBCs and controlled drug retention and releases from polymeric particles, we formulated RBCm-cloaked NPs in sub-100-nm sizes, which contained:
  - Sub-100-nm polymeric cores made from PLA or PLGA
  - An erythrocyte exterior made from RBCm with preserved membrane proteins
- *Drug loading efficiency:* We examined two distinct methods to load DOX as a model drug to the RBCm-cloaked NPs:
  - Physical encapsulation, resulting loading yields ranging from 0.9 wt% to 1.8 wt%
  - Covalent conjugation, resulting an approximate loading yield of 5 wt%
- *NP stability:* By monitoring NP sizes and UV absorbance, we found that RBCm-cloaked NPs had a superior stability when compared to bare polymeric cores without RBCm cloaks, implying that the RBCm cloak played a significant role in stabilizing NPs in biological solutions.

- *Sustained drug release:* Release studies showed drug-polymer covalent conjugation approach has a more sustained release profile than physical encapsulation, suggesting that the chemical linkers responsive to environmental triggers could achieve better-controlled drug releases when developing RBCm-cloaked NPs for advanced drug delivery applications.
- *Controlled drug release:* By comparing RBCm-cloaked NPs with PEGylated NPs, we found that RBCm acted as a diffusion barrier for DOX release. This observation was consistent with our quantitative analysis using Higuchi equations. Therefore, strategies aimed at engineering lipid membrane coatings can also enable responsive drug releases from RBCm-cloaked NPs under certain environmental cues.
- *Enhanced cytotoxicity:* DOX-loaded RBCm-cloaked NPs enhanced the efficacy against AML Kasumi-1 cells when compared to free DOX. This enhancement in efficacy can be likely attributed to endocytic uptake of NPs, which enables a high payload of drugs to enter the intracellular region.

Chapter 3, in full, is a reprint of the material as it appears in Nanomedicine 2013. Aryal, S.; Hu, C-M.; Fang, R.; Dehaini, D.; Carpenter, C.; Zhang, D-E.; Zhang L. are the co-authors of this material.

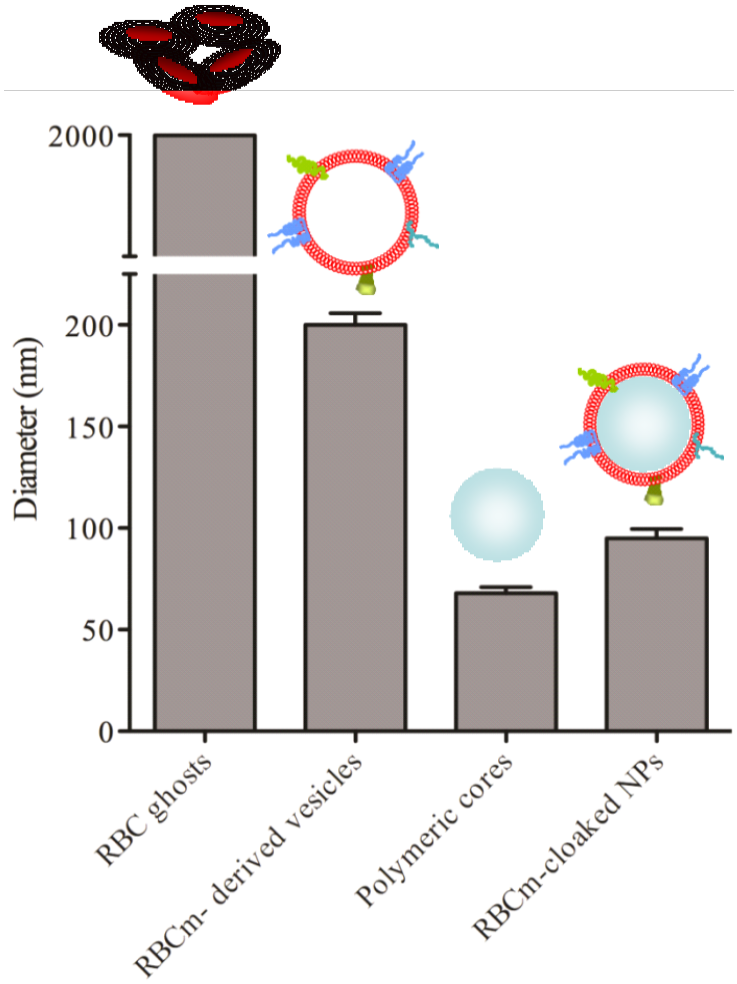

Figure 3.1. Schematic illustration of building materials and the preparation process of RBCm-cloaked NPs. The hydrodynamic size of RBC ghosts, RBCm-derived vesicles, polymeric cores, and RBCm-cloaked NPs were measured by DLS.

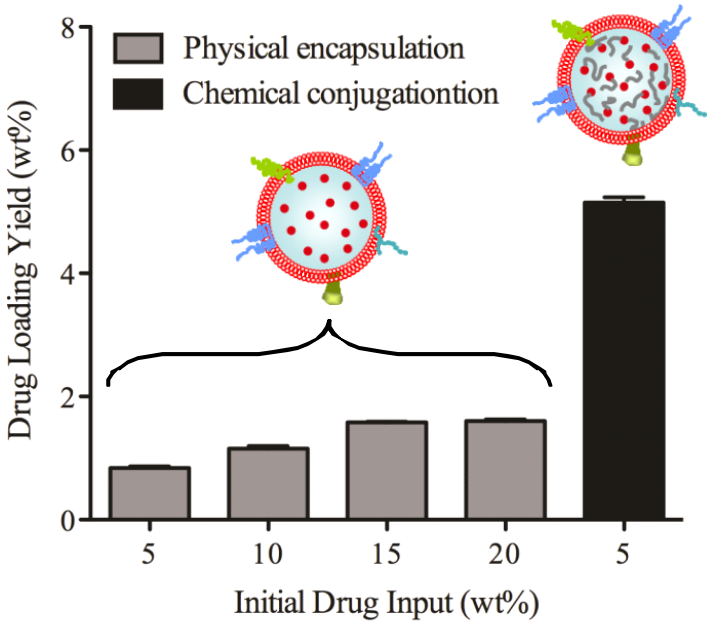

Figure 3.2. Doxorubicin (DOX) loading yields in the RBCm-cloaked NPs at various initial drug inputs. Drug molecules were loaded into the NPs through two distinct loading mechanisms: physical encapsulation and chemical conjugation, respectively.

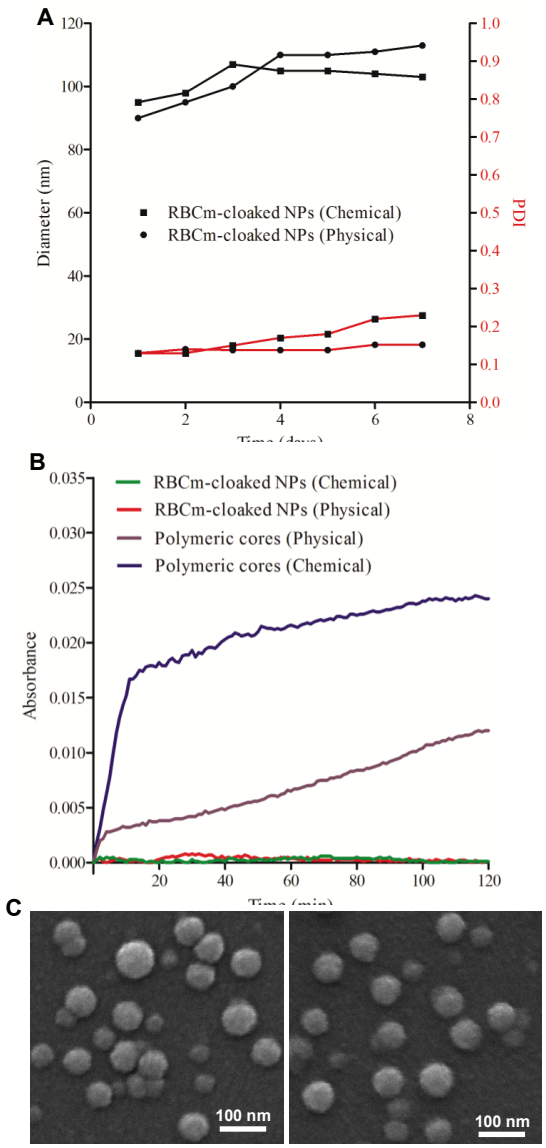

Figure 3.3. *In vitro* stability test and morphology of DOX-loaded RBCm-cloaked NPs. DOX was loaded into the NPs through either chemical conjugation or physical encapsulation. (A) Long-term stability of DOX-loaded RBCm-cloaked NPs in terms of particle size (diameter, nm) and polydispersity index (PDI) in PBS buffer, which were monitored for a period of 7 days at room temperature. (B) Stability of DOX-loaded RBCm-cloaked NPs and bare NP cores (without RBCm cloak) in 100% FBS was assessed by measuring the UV-absorbance at the wavelength of 560 nm. (C) Representative scanning electron microscope (SEM) images of DOX-loaded RBCm-cloaked NPs, of which the drugs were loaded through chemical conjugation (left) or physical encapsulation (right).

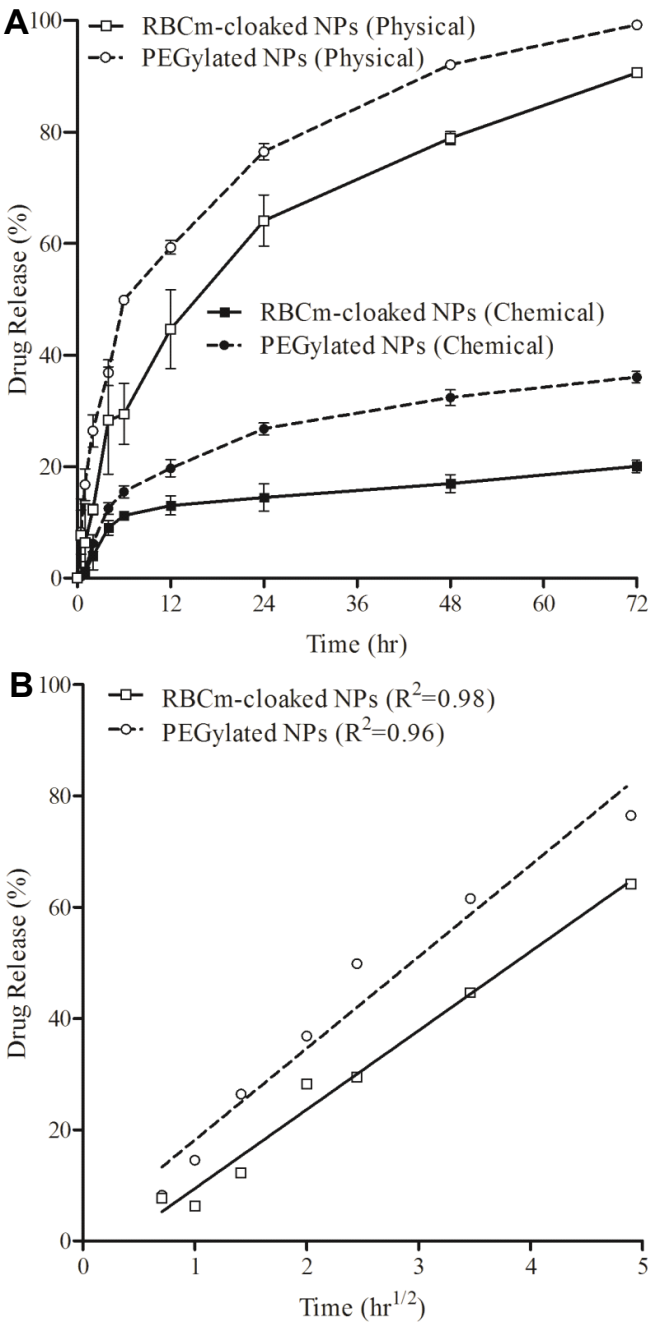

Figure 3.4. (A) DOX release profiles of RBCm-cloaked NPs and PEGylated NPs. For these release studies, initial DOX concentration inside the NPs was 5 wt% for chemical conjugation and 1.8 wt% for physical encapsulation, respectively. (B) For the physical encapsulation systems, the drug release percentage was plotted against the square root of time, which yielded linear fittings using a diffusion-dominant Higuchi model.

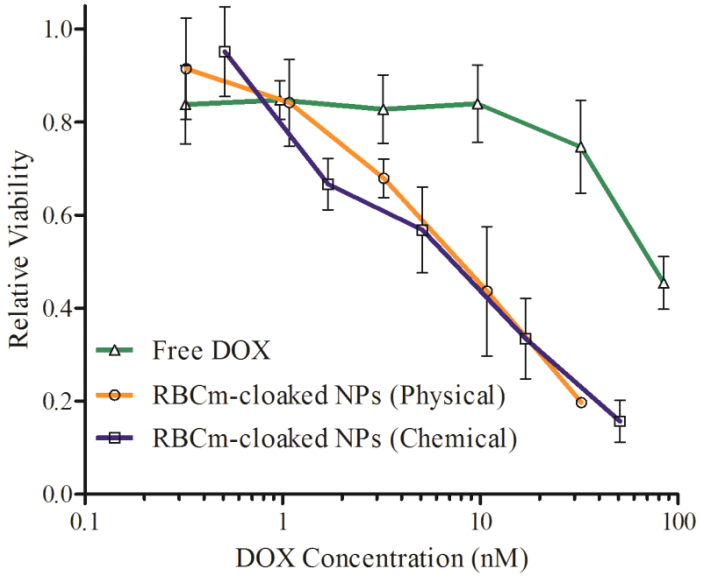

Figure 3.5. A comparative cytotoxicity study against Kasumi-1 cell line established from the peripheral blood of an AML patient, where squares represent RBCm-cloaked NPs with chemically conjugated DOX, circles represent RBCm-cloaked NPs with physically encapsulated DOX, and triangles represent free DOX. All samples were incubated with Kasumi-1 cells for 72 hours prior to MTT assay (n = 4).

3.6 References

1 Davis ME, Chen Z, Shin DM: Nanoparticle therapeutics: an emerging treatment modality for cancer. *Nat. Rev. Drug Discov.* 7(9), 771-782 (2008).

2 Petros RA, DeSimone JM: Strategies in the design of nanoparticles for therapeutic applications. *Nat. Rev. Drug Discov.* 9(8), 615-627 (2010).

3 Peer D, Karp JM, Hong S, FaroKhzad OC, Margalit R, Langer R: Nanocarriers as an emerging platform for cancer therapy. *Nat. Nanotechnol.* 2(12), 751-760 (2007).

4 Farokhzad OC, Langer R. Impact of Nanotechnology on Drug Delivery: *ACS Nano* 3(1), 16-20 (2009).

5 Alexis F, Pridgen E, Molnar LK, Farokhzad OC: Factors affecting the clearance and biodistribution of polymeric nanoparticles. *Mol. Pharm.* 5(4), 505-515 (2008).

6 Knop K, Hoogenboom R, Fischer D, Schubert US: Poly(ethylene glycol) in drug delivery: pros and cons as well as potential alternatives. *Angew. Chem. Int. Edit.* 49(36), 6288-6308 (2010).

7 Geng Y, Dalhaimer P, Cai S, Tsai R, Tewari M, Minko T, Discher DE.: Shape effects of filaments versus spherical particles in flow and drug delivery. *Nat. Nanotechnol.* 2(4), 249-255 (2007).

8 Yoo J-W, Chambers E, Mitragotri S: Factors that Control the Circulation Time of Nanoparticles in Blood: Challenges, Solutions and Future Prospects. *Curr. Pharm. Design* 16(21), 2298-2307 (2010).

9 Hu CM, Zhang L, Aryal S, Cheung C, Fang RH, Zhang L: Erythrocyte membrane-camouflaged polymeric nanoparticles as a biomimetic delivery platform. *Proc. Natl. Acad. Sci. USA* 108(27), 10980-10985 (2011).

10 Dodge JT, Mitchell C, Hanahan DJ: The preparation and chemical characteristics of hemoglobin-free ghosts of human erythrocytes. *Arch. Biochem. Biophys.* 100, 119-130 (1963).

11 Aryal S, Hu CM, Zhang L: Polymeric nanoparticles with precise ratiometric control over drug loading for combination therapy. *Mol. Pharm.* 8(4), 1401-1407 (2011).

12 Tong R, Cheng J: Ring-opening polymerization-mediated controlled formulation of polylactide-drug nanoparticles. *J. Am. Chem. Soc.* 131(13), 4744-4754 (2009).

13 Aryal S, Hu CM, Zhang L: Polymer--cisplatin conjugate nanoparticles for acid-responsive drug delivery. *ACS Nano* 4(1), 251-258 (2010).

14 Popielarski SR, Pun SH, Davis ME: A nanoparticle-based model delivery system to guide the rational design of gene delivery to the liver. 1. Synthesis and characterization. *Bioconjug. Chem.* 16(5), 1063-1070 (2005).

15 Fang RH, Aryal S, Hu CM, Zhang L: Quick synthesis of lipid-polymer hybrid nanoparticles with low polydispersity using a single-step sonication method. *Langmuir* 26(22), 16958-16962 (2010).

16 Tong R, Cheng J: Controlled Synthesis of Camptothecin-Polylactide Conjugates and Nanoconjugates. *Bioconjug. Chem.* 21(1), 111-121 (2010).

17 Gao W, Chan JM, Farokhzad OC: pH-Responsive Nanoparticles for Drug Delivery. *Mol. Pharm.* 7(6), 1913-1920 (2010).

18 Gu F, Zhang L, Teply BA *et al.*: Precise engineering of targeted nanoparticles by using self-assembled biointegrated block copolymers. *Proc. Natl. Acad. Sci. USA* 105(7), 2586-2591 (2008).

19 Takae S, Miyata K, Oba M *et al.*: PEG-detachable polyplex micelles based on disulfide-linked block catiomers as bioresponsive nonviral gene vectors. *J. Am. Chem. Soc.* 130(18), 6001-6009 (2008).

20 Zhang L, Chan JM, Gu FX *et al.*: Self-assembled lipid-polymer hybrid nanoparticles: A robust drug delivery platform. *ACS Nano* 2(8), 1696-1702 (2008).

21 Pornpattananangkul D, Zhang L, Olson S *et al.*: Bacterial Toxin-Triggered Drug Release from Gold Nanoparticle-Stabilized Liposomes for the Treatment of Bacterial Infection. *J. Am. Chem. Soc.* 133(11), 4132-4139 (2011).

22 Avgoustakis K, Beletsi A, Panagi Z, Klepetsanis P, Karydas AG, Ithakissios DS: PLGA-mPEG nanoparticles of cisplatin: in vitro nanoparticle degradation, in vitro drug release and in Vivo drug residence in blood properties. *J. Control. Release* 79(1-3), 123-135 (2002).

23 Li J, Jiang G, Ding F: The effect of pH on the polymer degradation and drug release from PLGA-mPEG microparticles. *J. Appl. Polym. Sci.* 109(1), 475-482 (2008).

24 Higuchi T: Rate of release of medicaments from ointment bases containing drugs in suspension. *J. Pharm. Sci.* 50, 874-875 (1961).

25 Siepmann J, Peppas NA: Higuchi equation: derivation, applications, use and misuse. *Int. J. Pharm.* 418(1), 6-12 (2011).

26 Budhian A, Siegel SJ, Winey KI: Controlling the in vitro release profiles for a system of haloperidol-loaded PLGA nanoparticles. *Int. J. Pharm.* 346(1-2), 151-159 (2008).

27 Pitt CG, Schindler A: The kinetics of drug cleavage and release from matrices containing covalent polymer-drug conjugates. *J. Control. Release* 33(3), 391-395 (1995).

28 Lowenberg B, Ossenkoppele GJ, van Putten W *et al.*: High-Dose Daunorubicin in Older Patients with Acute Myeloid Leukemia. *New Engl. J. Med.* 361(13), 1235-1248 (2009).

29 Hu C-MJ, Zhang L: Therapeutic Nanoparticles to Combat Cancer Drug Resistance. *Curr. Drug Metab.* 10(8), 836-841 (2009).

30 Ayen WY, Garkhal K, Kumar N: Doxorubicin-loaded $(PEG)_3$-PLA nanopolymersomes: effect of solvents and process parameters on formulation development and in vitro study. *Mol. Pharm.* 8(2), 466-478 (2011).

31 Yoo HS, Park TG: Folate-receptor-targeted delivery of doxorubicin nano-aggregates stabilized by doxorubicin-PEG-folate conjugate. *J. Control. Release* 100(2), 247-256 (2004).

32 Huwyler J, Cerletti A, Fricker G, Eberle AN, Drewe J. By-passing of P-glycoprotein using immunoliposomes. *J. Drug Target.* 10(1), 73-79 (2002).

33 Rapoport N, Marin A, Luo Y, Prestwich GD, Muniruzzaman M. Intracellular uptake and trafficking of pluronic micelles in drug-sensitive and MDR cells: Effect on the intracellular drug localization. *J. Pharm. Sci.* 91(1), 157-170 (2002).

34 Sahoo SK, Labhasetwar V. Enhanced anti proliferative activity of transferrin-conjugated paclitaxel-loaded nanoparticles is mediated via sustained intracellular drug retention. *Mol. Pharm.* 2(5), 373-383 (2005).

35 Dordal MS, Jackson-Stone M, Ho AC, Winter JN, Atkinson AJ: Decreased intracellular compartmentalization of doxorubicin in cell lines expressing P-glycoprotein. *J. Pharmacol. Exp. Ther.* 271(3), 1286-1290 (1994).

4 Lipid-insertion enables targeting functionalization of erythrocyte membrane-cloaked nanoparticles

*Nanoscale 2013

4.1 Introduction

A major goal in engineering nanocarriers for systemic drug delivery is to achieve long circulation half-lives,[1] as increased residence time in the bloodstream can improve the pharmacokinetic profile of therapeutic cargoes and allow a greater chance for the nanocarriers to reach the desired location through either passive[2, 3] or active[4-6] targeting mechanisms. Ongoing search for new and effective ways to construct long-circulating nanoparticles has introduced numerous stealth functionalization strategies. While the use of synthetic polymers represents the current golden standard for prolonging particle residence time in circulation, recent efforts have drawn inspiration from nature to bestow immune-evasive properties on nanoparticles.[7, 8] Bridging the complex surface biochemistry of nature's carriers, RBCs, with the versatile cargo-carrying capacity of polymeric nanoparticles, an RBC membrane-cloaked nanoparticle (RBC-NP) platform represents a new class of bio-inspired nanocarriers with long-circulating capability.[9, 10] In this system, a top-down approach is used to coat polymeric nanoparticles with natural RBC membranes, which possess a litany of immunomodulatory proteins responsible for RBCs' extraordinarily long survival in circulation.[11-14] This membrane cloak acts to camouflage the nanoparticle *in vivo* to evade immune attacks.[9] Consisting entirely of biocompatible and biodegradable materials, the RBC-NPs have significant potential for drug delivery applications.

In applying RBC-NPs for disease treatments, particularly against cancers, target-selectivity is a desirable feature that promises minimization of off-target side effects.[15-19] Cancer targeting has been made possible by carrier functionalization with ligands that target overexpressed tumor antigens, and numerous chemical conjugation techniques employing carboxyl-, amine-, or sulfhydryl-based chemistry have been used to decorate synthetic nanocarriers with targeting ligands.[20-26] In the case of biologically derived carriers such as RBC-NPs, however, the presence of biological components on the particle surfaces demands a non-disruptive functionalization strategy since the immune evasion capabilities of cellular membranes is predicated upon having fully functional proteins. In order to address the issue of chemical denaturation, we report a lipid-insertion approach to functionalizing RBC-NPs that exploits the fluidity of bilayered RBC lipid membranes and precludes RBC membrane exposure to chemical reactions. As shown in Fig. 1, targeting moieties are incorporated onto RBC membranes through the aid of lipid tethers. The physical insertion of ligand-linker-lipid conjugates into the RBC membranes produces functionalized RBC membranes without damaging the existing surface proteins. Using two differently sized ligands, a small molecule folate (MW ~ 441 Da) and a nucleolin-targeting aptamer AS1411 (MW ~ 9,000 Da), we demonstrate that the lipid-insertion technique can be applied to targeting ligands of different length scales. Following preparation of RBC-NPs with the functionalized RBC membranes, their receptor-specific targeting ability is verified in model cancer cell lines *in vitro*.

Results and Discussion

To demonstrate that lipid-tethered ligands can be spontaneously incorporated onto RBC membranes, a FITC-linker-lipid (excitation/emission = 495/519 nm) conjugate was

used for a proof-of-concept test, where FITC was linked to a lipid molecule through a short polyethylene glycol chain (MW ~ 2,000 Da). In the study, 40 μg of FITC-PEG-lipid was first incubated with emptied red blood cells (RBC ghosts) collected from 1 mL of whole mouse blood for 30 min. The RBC ghosts were then centrifuged, washed with PBS, reconstituted, and examined using flow cytometric analysis (Fig. 2A). Compared to unmodified RBC ghosts, modified membrane ghosts had significantly higher signal under the FITC channel. Visualization by fluorescence microscopy further confirmed the localization of the lipid-tethered FITC on the RBC membranes, as the microscopy image displays strong FITC signals outlining the exterior of the RBC ghosts (Fig. 2B). To characterize the lipid-insertion efficiency and saturation, varying amounts of FITC-PEG-lipid were incubated with the membrane ghosts followed by membrane purification through centrifugation. Fluorescence quantification showed that the retained FITC fluorescence increased with the initial FITC-PEG-lipid input (Fig. 2C). Saturation was observed as the retained FITC-PEG-lipid approached a plateau at approximately 40 μg per mL of RBCs. Based on the RBC concentration and the molecular weight of the ligand, it is estimated that each RBC ghost contains about 800,000 FITC-PEG-lipid. Fig. 2C also demonstrates adjustability of ligand density on the membranes by controlling the lipid-tethered ligand input.

Upon confirming the incorporation of FITC onto the RBC ghosts, the membrane materials were then used to prepare FITC-modified RBC-NPs. Following a previously reported protocol,[9] the FITC-modified RBC membrane ghosts were extruded to form ~100 nm vesicles, which were then mixed and extruded with 70 nm PLGA particles to generate FITC-modified RBC-NPs. For comparison, RBC-NPs coated with unmodified

RBC membranes were also prepared. Characterization of the two particles by dynamic light scattering (DLS) showed similar physicochemical properties between the FITC-modified and unmodified RBC-NPs (Fig. 2D). Both particles were approximately 80 nm in mean diameter and under -25 mV in zeta potential. Scanning electron microscopy (SEM) further demonstrated the similarity between the two particle types (Fig. 2E), both of which were spherical in morphology and exhibited monodisperse population distributions. To confirm the colocalization of lipid-tethered ligands with the polymeric cores, an *in vitro* fluorescence colocalization study was conducted by loading DiD dye (excitation/emission = 644/663 nm) into the polymeric cores. Following cellular uptake, significant overlap was observed between the DiD-specific red punctates and the FITC-specific green punctates (Fig. 2F). The colocalization pattern confirms the presence of lipid-tethered FITC on the surface of the polymeric cores, demonstrating successful preparation of ligand-modified RBC-NPs.

After validating the lipid-insertion method for RBC-NP functionalization using lipid-tethered fluorescent probes, particle modification with cancer-targeting ligands was explored. A small molecule ligand, folate (MW ~ 441 Da), which has similar molecular weight as FITC, was first examined. Folate-functionalized nanocarriers have broad applicability as folate receptors are overexpressed on several types of cancers.[27] Upon receptor-mediated binding, folate-functionalized nanocarriers can deliver their cargoes intracellularly through an endocytic uptake pathway. The benefit of folate-induced cancer targeting has been demonstrated on several nanocarrier platforms,[28, 29] and thus its incorporation onto RBC-NPs can improve the particles' utility in cancer drug delivery.

To prepare folate-functionalized RBC-NPs, a commercially available folate-PEG-

lipid conjugate was used (Fig. 3A). Folate-functionalized RBC-NPs were prepared using RBC ghosts inserted with folate-PEG-lipid. Since the targeting ability of folate-functionalized nanoparticles has already been well-established, the KB cell line, a model cancer cell line overexpressing the folate receptor that is commonly used to evaluate folate targeting,[30-32] was used to confirm successful functionalization of the RBC-NPs. To assess for folate-mediated differential uptake, the cells were cultured in folate-free media and incubated with folate-functionalized RBC-NPs, non-targeted RBC-NPs, or folate-functionalized RBC-NPs together with 1 mM of free folate. The cells from each sample were then detached, washed, and analyzed using flow cytometry (Fig. 3B,C). Compared to the non-targeted RBC-NPs, the particles functionalized with folate ligand resulted in an 8-fold increase in cellular uptake. Conjoint incubation with folate-functionalized RBC-NPs and 1 mM of free folate yielded a similar level of cellular uptake as compared to non-targeted RBC-NPs, which indicates that the increased uptake of folate-functionalized RBC-NPs was receptor-specific. Fluorescence microscopy visualization of particle uptake further confirmed the results observed from flow cytometry. As shown in Fig. 3D, fluorescence from the DiD dye encapsulated inside the particles was only observed in cells incubated with folate-functionalized RBC-NPs in the absence of free folate molecules. To demonstrate that the targeting effects were exclusive to cells overexpressing the folate receptor, a negative cancer cell line[33], A549, was incubated with either unmodified or folate-functionalized RBC-NPs. No increased uptake was observed for the targeted nanoparticles compared to the unmodified nanoparticles using both flow cytometry and fluorescence imaging (ESI Fig. S1A,B†). Important to note also is that no cytotoxicity was observed for the RBC-NPs when incubated with

human umbilical vein endothelial cells (HUVECs), a normal cell line, at the concentrations used in these studies (ESI Fig. S2†). Overall, the results confirm the receptor-specific targeting capability of folate-functionalized RBC-NPs.

To demonstrate that the lipid-insertion method can be applied to targeting ligands of different length scales, a nucleolin-targeting oligonucleotide, AS1411 aptamer (MW ~ 9,000 Da), was also tested for particle functionalization. Oligonucleotide-based targeting agents, or aptamers, are a versatile class of ligands that can be customized against specific receptors through affinity screening.[34] AS1411, a 26-mer DNA aptamer with the sequence GGT GGT GGT GGT TGT GGT GGT GGT GG, has shown targeting capability against several cancer cell types owing to frequent overexpression of surface nucleolin on cancerous cells.[35-37] The ligand has also been applied for the preparation of cancer-targeted nanoparticles,[38, 39] thus its integration onto the RBC-NPs would greatly benefit the utility of the platform.

To incorporate aptamers onto RBC-NPs via lipid-insertion, a lipid-tethered AS1411 was first prepared. AS1411 aptamers containing a 3' thiol modifier was reduced using tris[2-carboxyethyl]phosphine (TCEP) and conjugated to lipid-PEG-maleimide via maleimide-sulfhydryl chemistry (Fig. 4A). After purification, the AS1411-PEG-lipid conjugates were used to prepare RBC-NPs following the aforementioned procedures. In a cellular uptake study using a surface nucleolin expressing breast cancer cell line, MCF-7,[35] differential targeting was observed. Flow cytometry analysis revealed that the targeted nanoparticles induced a two-fold increase in cellular uptake as compared to the non-targeted RBC-NPs (Fig. 4B,C). The uptake enhancement by the targeted nanoparticles was also confirmed to be receptor-specific, as blocking by free AS1411

reduced the particle uptake to the level of the non-targeted nanoparticles. Fluorescence imaging corroborated the flow cytometry results with the AS1411-fuctionalized RBC-NP showing much greater uptake than the non-targeted and blocked samples (Fig. 4D). The results demonstrate that the lipid-insertion method can be applied to relatively large targeting ligands (e.g., MW ~ 9,000 Da) with a molecular weight larger than that of the lipid anchor (MW ~ 748 Da).

4.2 Conclusions

In summary, by employing a lipid-insertion technique for the functionalization of biological membrane, targeted RBC-NPs were successfully prepared with two different types of targeting ligands. Through the aid of lipid tethers and the dynamic conformation of membrane bilayers, targeting ligands can be spontaneously incorporated onto the RBC-NP platform without exposing the biological membranes to chemical reactions. The robustness and simplicity of this functionalization scheme can enable a wide array of functionalized RBC-NPs for specific disease treatments. In addition, the technique can be generalized to help improve the applicability of emerging biologically inspired nanocarriers possessing complex surface chemistry. The capability to control and adjust ligand density through the lipid-insertion technique also provides versatility for platform optimization. Future studies are warranted to examine the *in vivo* implications of ligand functionalization on RBC-NPs. The targeted RBC-NPs reported in the present work possess significant potential for cancer treatments as they integrate nature's immune-evasive moieties with cancer-binding ligands.

Chapter 4, in full, is a reprint of the material as it appears in Nanoscale 2013. Fang, R.; Hu, C-M.; Chen, K.; Luk, B.; Carpenter, C.; Gao, W.; Li, S.; Zhang, D-E.; Lu,

W.; Zhang, L. are the co-authors of this material.

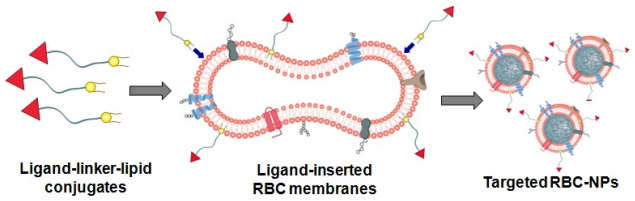

Figure 4.1. Schematic of the preparation of RBC-NPs with targeting ability. Ligand-linker-lipid conjugates are synthesized and then inserted into RBC membrane ghosts. The resulting ligand-functionalized RBC membranes are used to coat polymeric cores to form targeted RBC-NPs.

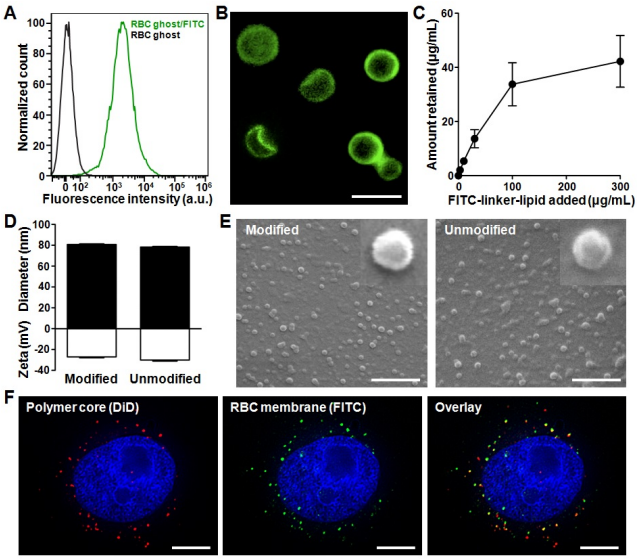

Figure 4.2. Lipid-insertion enables modification of RBC-NPs with FITC. (A) Flow cytometry histograms of plain RBC ghosts (black) and RBC ghosts incorporated with FITC-linker-lipid (green). (B) Fluorescence microscopy visualization of RBC ghosts modified with FITC (green). Scale bar = 8 μm. (C) FITC-linker-lipid was incubated with RBC ghosts derived from 1 mL of mouse blood. The amount of FITC-linker-lipid incorporated onto the RBC ghosts was then quantified after 30 min of incubation and plotted against the initial input. (D) Physicochemical characterizations (size and zeta potential) of both FITC-modified and unmodified RBC-NPs. (E) SEM images of FITC-modified and unmodified RBC-NPs. Insets represent a single particle with a size of ~80 nm. Scale bars = 500 nm. (F) Colocalization of the polymeric core (red) and the FITC-modified RBC membrane shell (green) upon intracellular uptake by KB cells. Cellular nuclei were stained with DAPI (blue). Scale bars = 8 μm.

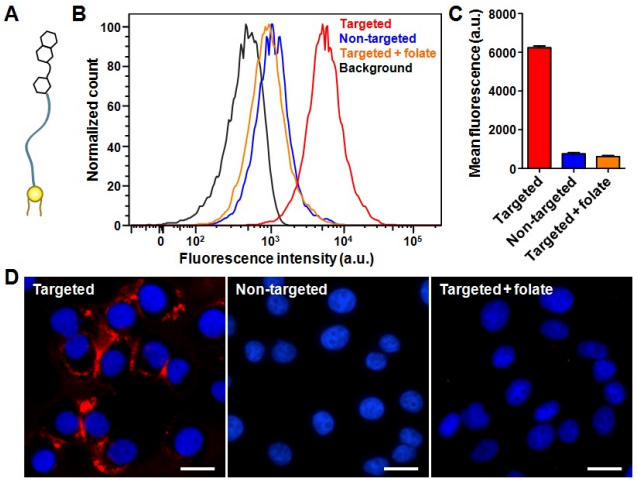

Figure 4.3. Lipid-insertion enables targeting functionalization of RBC-NPs with folate. (A) Schematic representation of folate-linker-lipid. (B) Flow cytometry histograms of KB cells alone (black) and the cells incubated with folate-functionalized RBC-NPs (red), non-targeted RBC-NPs (blue), and folate-functionalized RBC-NPs together with free folate (orange). (C) Quantification of the mean fluorescence intensity of the histograms in (B). (D) Fluorescence microscopy of KB cells incubated with folate-functionalized RBC-NPs, non-targeted RBC-NPs, and folate-functionalized RBC-NPs together with free folate. A fluorescent probe DiD was loaded inside the RBC-NPs for visualization (red) and cellular nuclei were stained with DAPI (blue). Scale bars = 25 μm.

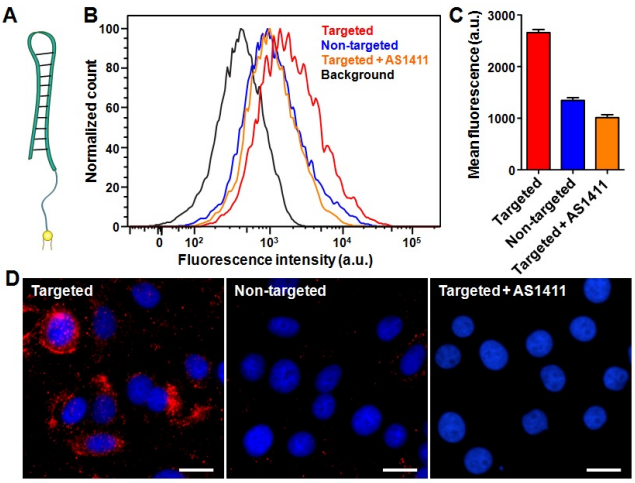

Figure 4.4. Lipid-insertion enables targeting functionalization of RBC-NPs with AS1411 aptamer. (A) Schematic representation of AS1411-linker-lipid. (B) Flow cytometry histograms of MCF-7 cells alone (black) and the cells incubated with AS1411-functionalized RBC-NPs (red), non-targeted RBC-NPs (blue), and AS1411-functionalized RBC-NPs together with free AS1411 aptamer (orange). (C) Quantification of the mean fluorescence intensity of the histograms in (B). (D) Fluorescence microscopy of MCF-7 cells incubated with AS1411-functionalized RBC-NPs, non-targeted RBC-NPs, and AS1411-functionalized RBC-NPs together with free AS1411. A fluorescent probe DiD was loaded inside the RBC-NPs for visualization (red) and cellular nuclei were stained with DAPI (blue). Scale bars = 25 μm.

4.3 References

1 S. D. Li, L. Huang, *Mol. Pharm.,* 2008, 5, 496-504.

2 H. Maeda, J. Wu, T. Sawa, Y. Matsumura, K. Hori, *J. Control. Release,* 2000, 65, 271-284.

3 A. K. Iyer, G. Khaled, J. Fang, H. Maeda, *Drug Discov. Today,* 2006, 11, 812-818.

4 R. Singh, J. W. Lillard, Jr., *Exp. Mol. Pathol.,* 2009, 86, 215-223.

5 D. F. Emerich, C. G. Thanos, *J. Drug Target.,* 2007, 15, 163-183.

6 L. Brannon-Peppas, J. O. Blanchette, *Adv. Drug Deliv. Rev.,* 2004, 56, 1649-1659.

7 R. H. Fang, C. M. Hu, L. Zhang, *Expert Opin. Biol. Ther.,* 2012, 12, 385-389.

8 C. M. Hu, R. H. Fang, L. Zhang, *Adv. Healthcare Mater.,* 2012, 1, 537-547.

9 C. M. Hu, L. Zhang, S. Aryal, C. Cheung, R. H. Fang, L. Zhang, *Proc. Natl. Acad. Sci. USA,* 2011, 108, 10980-10985.

10 C. M. Hu, R. H. Fang, J. Copp, B. T. Luk, L. Zhang, *Nat. Nanotechnol.*, 2013, 8, 336-340.

11 D. D. Kim, W. C. Song, *Clin. Immunol.,* 2006, 118, 127-136.

12 P. A. Oldenborg, A. Zheleznyak, Y. F. Fang, C. F. Lagenaur, H. D. Gresham, F. P. Lindberg, *Science,* 2000, 288, 2051-2054.

13 R. K. Tsai, D. E. Discher, *J. Cell. Biol.,* 2008, 180, 989-1003.

14 R. K. Tsai, P. L. Rodriguez, D. E. Discher, *Blood Cell Mol. Dis.,* 2010, 45, 67-74.

15 O. C. Farokhzad, R. Langer, *Adv. Drug Deliv. Rev.,* 2006, 58, 1456-1459.

16 M. E. Davis, Z. Chen, D. M. Shin, *Nat. Rev. Drug Discov.,* 2008, 7, 771-782.

17 D. Peer, J. M. Karp, S. Hong, O. C. Farokhzad, R. Margalit, R. Langer, *Nat. Nanotechnol.,* 2007, 2, 751-760.

18 V. Wagner, A. Dullaart, A. K. Bock, A. Zweck, *Nat. Biotechnol.,* 2006, 24, 1211-1217.

19 L. Zhang, F. X. Gu, J. M. Chan, A. Z. Wang, R. S. Langer, O. C. Farokhzad, *Clin. Pharmacol. Ther.,* 2008, 83, 761-769.

20 K. C. R. Bahadur, B. Thapa, P. S. Xu, *Mol. Pharm.,* 2012, 9, 2719-2729.

21 D. Bartczak, A. G. Kanaras, *Langmuir,* 2011, 27, 10119-10123.

22 T. Chen, I. Ocsoy, Q. Yuan, R. W. Wang, M. X. You, Z. L. Zhao, E. Q. Song, X. B. Zhang, W. H. Tan, *J. Am. Chem. Soc.,* 2012, 134, 13164-13167.

23 C. M. Hu, S. Kaushal, H. S. T. Cao, S. Aryal, M. Sartor, S. Esener, M. Bouvet, L. Zhang, *Mol. Pharm.,* 2010, 7, 914-920.

24 E. L. Jin, B. Zhang, X. R. Sun, Z. X. Zhou, X. P. Ma, Q. H. Sun, J. B. Tang, Y. Q. Shen, E. Van Kirk, W. J. Murdoch, M. Radosz, *J. Am. Chem. Soc.,* 2013, 135, 933-940.

25 M. M. J. Kamphuis, A. P. R. Johnston, G. K. Such, H. H. Dam, R. A. Evans, A. M. Scott, E. C. Nice, J. K. Heath, F. Caruso, *J. Am. Chem. Soc.,* 2010, 132, 15881-15883.

26 J. Wang, S. M. Tian, R. A. Petros, M. E. Napier, J. M. DeSimone, *J. Am. Chem. Soc.,* 2010, 132, 11306-11313.

27 J. Sudimack, R. J. Lee, *Adv. Drug Deliv. Rev.,* 2000, 41, 147-162.

28 X. Pan, R. J. Lee, *Expert Opin. Drug Deliv.,* 2004, 1, 7-17.

29 J. D. Byrne, T. Betancourt, L. Brannon-Peppas, *Adv. Drug Deliv. Rev.,* 2008, 60, 1615-1626.

30 R. J. Lee, P. S. Low, *J. Biol. Chem.,* 1994, 269, 3198-3204.

31 R. J. Lee, P. S. Low, *BBA-Biomembranes,* 1995, 1233, 134-144.

32 S. Wang, R. J. Lee, G. Cauchon, D. G. Gorenstein, P. S. Low, *Proc. Natl. Acad. Sci. USA,* 1995, 92, 3318-3322.

33 H. S. Yoo, T. G. Park, *J. Control. Release,* 2004, 100, 247-256.

34 G. Mayer, M. S. L. Ahmed, A. Dolf, E. Endl, P. A. Knolle, M. Famulok, *Nat. Protoc.,* 2010, 5, 1993-2004.

35 S. Soundararajan, W. W. Chen, E. K. Spicer, N. Courtenay-Luck, D. J. Fernandes, *Cancer Res.,* 2008, 68, 2358-2365.

36 F. Mongelard, P. Bouvet, *Curr. Opin. Mol. Ther.,* 2010, 12, 107-114.

37 S. Soundararajan, L. Wang, V. Sridharan, W. W. Chen, N. Courtenay-Luck, D. Jones, E. K. Spicer, D. J. Fernandes, *Mol. Pharm.,* 2009, 76, 984-991.

38 A. Aravind, P. Jeyamohan, R. Nair, S. Veeranarayanan, Y. Nagaoka, Y. Yoshida, T. Maekawa, D. S. Kumar, *Biotechnol. Bioeng.,* 2012, 109, 2920-2931.

39 D. W. Hwang, H. Y. Ko, J. H. Lee, H. Kang, S. H. Ryu, I. C. Song, D. S. Lee, S. Kim, *J. Nucl. Med.,* 2010, 51, 98-105.